AALTO UNIVERSITY,
SCHOOL OF SCIENCE
Master's Programme in Advanced Materials

Magnetic Strength Compatibilization of Soft Magnetic Composites using a Magnetic Force Sensing Device

Maximilian de Rozières Gentilhomme de Laveline

Master's Thesis

Espoo, July 31, 2020

Supervisor: Jaakko Timonen, Assistant Professor

Thesis Advisor: Meri Lundahl, Head of Material Innovations at Teraloop Oy

Abstract

In this thesis, Fe-based Soft Magnetic Composites (SMC) varying in thermoset resins are prepared using a variety of metallurgical techniques. Their magnetic properties are then studied, tested, then compared with each other. Three various resins were used for specimen preparation: Biresin CR131, G/Flex, and Biothan. The magnetic pull strength between the SMC samples and a permanent magnet (PM) was measured, with respect to each other's distances, using a device I built entirely with limited resources available. This device is called a magnetic force sensor (MFS). The details and methodology used to construct this device will be clearly described within this paper. A finite element method software is used to compare and validate the credibility of the MFS. The outcome proves to corroborate my device's capabilities as a credible tool for research. Of the SMC experiments taken with the device, resin base CR131 showed the strongest magnetic response to the PM while Biothan showed the weakest response. The quality of SMC due to preparation will be a key topic of my results and discussion.

Preface

This Master's thesis is based on the work performed with the company Teraloop Oy in collaboration with the School of Science at Aalto University, between January-July 2020. The project has been carried out under the supervision of Vice Head of Department of Applied Physics and Assistant Professor Jaakko Timonen and Head of Material Innovations for Teraloop and Postdoctoral Researcher at Aalto Department of Bioproducts and Biosystems Dr. Meri Lundahl.

First and foremost, I would like to thank Meri Lundahl for being the first to accept the responsibility of being my advisor. Her help throughout this thesis process cannot be praised enough. I would like to thank Jaakko Timonen for as well taking on the responsibility of being my supervisor. His knowledge in magnetism is profound and now so is mine. I would like to thank the Teraloop team for accepting me into their family and teaching me everything there is to know on flywheel technology. A big thank you to Roozbeh Abidnejad for teaching/helping me with so much throughout my time working on the thesis and for putting up with my craziness. His support throughout has meant a lot. Of course, I would like to thank the Advanced Materials in Innovation and Sustainability (AMIS) program headed by the European Institute of Technology (EIT) for accepting me into their program and for as well supporting me throughout my education. Lastly, a big thank you to friends and family for loving me for who I am. Without my mother, brother, and father none of this would have happened.

Table of Contents

List of Acronyms

Abbreviations

SMC	Soft magnetic composite
MFS	Magnetic force sensor device
PM	permanent magnet
FEM	Finite element method
AFM	Antiferromagnetic material
SEM	scanning electron microscopy
SMM	Soft magnetic materials
CGS	Centimeter-gram-second
2D	two-dimensional
3D	three-dimensional
DC	direct current
AC	alternating current
AI	artificial intelligence
Fe	Iron

Symbols

F	Force
F_V	Force per unit volume
ρ	charge density
k_e	Coulomb's constant
μ_0	magnetic permeability
E	electric field
B	magnetic flux density
H	magnetic field strength
M	magnetization
χ	magnetic susceptibility
μ_B	Bohr Magneton
S	electron spin
h	Planck’s constant

g_s	g-factor
T_c	Curie temperature
T_N	Neel temperature
τ	torque
μ	magnetic dipole moment
J	angular momentum vector
γ	gyromagnetic ratio
ω	angular frequency
E	energy
K	magnetic anisotropy constant
H_c	coercive force
J_s	saturation polarization
P_h	Hysteresis loss
P_e	Eddy current loss
P_r	Residual loss
P	Porosity

Equations

[1]. Coulomb force
[2]. Magnetic field of a moving charge
[3]. Lorentz force
[4]. Magnetic force with relation to area
[5]. Magnetic moment of an electron
[6]. Energy stored in a magnetic field
[7]. Magnetization with respect to susceptibility and applied magnetic field
[8]. Torque of a body exerted by applied magnetic field
[9]. Larmor frequency
[10]. Energy required to rotate the magnetization
[11]. Permeability in relation to field strength and flux density
[12]. Relative permeability with respect to size of particle
[13]. Hysteresis loss
[14]. Eddy current loss

1. Introduction

Research and development for any product is a process that is highly dependent on laboratories. These institutions can house quality equipment totaling in the ranges of upwards a million dollars, which are used to further the scientific endeavors that will one day benefit the standard of living for the global population. These laboratories tend to be used by a large density of students/professionals in pursuit of advancing their research topic. However, what happens when the laboratories are forced to close due to an unforeseen event? Then the advancement of science, and arguably that of humanity, would cease to progress. This seemingly impossible scenario has become reality due to the COVID-19 pandemic of 2020.

The unforeseen global crisis caused by the pandemic of 2020 has tested our abilities to adapt and work towards a means of furthering research, while many alternative solutions are left inaccessible. To decrease the spread of this infectious disease, governments around the world have closed down any institution that may house a large number of human interactions: including laboratories. The closing of laboratories has greatly impacted those whose research and degrees are heavily dependent on the devices required to test, record, and elucidate their results. This thesis, for one, is to be considered as a demonstration of how one can persevere during trying times and still achieve scientific results.

Teraloop Oy is a next generation flywheel technology-based company, whose focus is to construct a grid-scale energy storage system that can sustainably service a wide range of different markets. Their work consists of an old technology, but one now reinvigorated as a plausible solution for many energy storage applications thanks to modern discoveries in material science. Flywheels act as an energy storage device (battery), which functions through kinetic motion rather than electrochemical reactions. However, unlike electrochemical reactions such as lithium ion batteries, flywheels have proven to be more advantageous in many regards. Some

advantages include faster charge and discharge time, longer life span, less maintenance, versatility in implementation/size, and environmentally sustainable to list a few.

Although kinetic energy storage flywheels have been a well-established concept for centuries, it is only recently that their storage capabilities have been taken to new heights. These great new heights are all thanks to the advancements made in material science. The discovery of materials such as fiber composites (i.e. carbon fiber) have provided a means of replacing aluminum steel as material of choice for the rotor. Thanks to its high tensile strength to density ratio, fiber-based composites provide a far superior means of storing a high specific energy due to its capabilities of spinning at uncanny speeds. In addition to the benefits of using carbon fiber, was how magnetism changed the design completely. While harnessing magnetism, one could magnetically levitate the rotor so that there is little to no friction. With less friction now, new generation flywheels are capable of spinning with speeds up to 5000km/h (42) and become more economically viable. However, for the rotor to function properly and efficiently so that it can reach such speeds, it needs supporting parts which can sustain high temperatures. In order to minimize electromagnetic losses, which will be described further in this paper, from heat dissipation of the rim in the form of radiation, a soft magnetic composite (SMC) is used for the rotors of the active magnetic bearings. Hence, SMC plays an important role in the integration of flywheel technology for eventual application leading to a benefit for the global population. The work provided within this paper revolves heavily around SMC material theory, preparation, production, current problems, and possible solutions. Additionally, the possibility to construct a low cost and effective device that can measure the magnetic properties of my SMC samples was investigated.

The device is called the magnetic force sensor (MFS), which was built in response to the closure of laboratories. The MFS's capabilities are limited to only measuring the magnetic force (in grams) while approached at certain distances from a rare-earth permanent magnet (PM). To corroborate the effectiveness of my device, a material with well-known properties was used for preliminary tests where the results from both the device and theoretical ones were compared. A

finite element method software was used to simulate theoretical values for comparison. Matching values would prove the success of my device, which would then allow further measurements to be done to my SMC samples. SMC samples were prepared using various established techniques and will be a key topic of this paper. Different epoxy resins, which are a staple material in SMC, were implemented while preparing different samples. The trade names of these resins are: Biresin CR131, G/Flex, and Biothan. The differences between these resins used in the SMC samples were studied, tested, plotted, and compared in respect to their response with my MFS device. The objective was to see the effect varying resins have onto the magnetic properties of our samples and to study how sample preparation can ultimately affect this outcome as well.

2. Literature review

2.1 Magnetism and Magnetic properties

2.1.1 Fundamental properties of Electromagnetism

Many fundamental/subatomic particles of matter carry a quantized characteristic property known as an electric charge, which are of two general types: positive or negative. A direct and convincing measurement of an electric charge, as a natural unit, was first made (1909) in the Millikan oil-drop experiment where both the amount of electric force and magnitude of electric field on a tiny charge of an isolated droplet was measured (11). Subatomic particles while stationary will produce an electric field due to their electric charge. This electric field induces a force onto other particles resulting in either a net attraction or repulsion, depending on the particle's affinity. Like charges will repel while opposites will attract. This force is conventionally called the electrostatic force or Coulomb force, represented by:

$$F = k_e \frac{q_1 q_2}{r^2},$$

[1]

Where F is force, k_e is Coulomb's constant ($k_e = 9 \times 10^9 \frac{Nm^2}{C^2}$), q_1 and q_2 are the charges with their respective signs, and r is the scalar distance between charges. Magnetism is the result of electric charges in motion, due to the Coulomb force, and mediated by magnetic fields. The magnetic field of a moving charge can be expressed as

$$\mathrm{B} = \frac{\mu_0}{4\pi}\frac{\mathrm{qv}\times\mathrm{r}}{\mathrm{r}^2} \qquad [2]$$

Where ($\mu_0 = 4\pi \times 10^{-7} \frac{Ns^2}{C^2}$)is called the permeability of free space, q is the charge, r is distance, and v is the charge's velocity.

The forces produced by a magnet that act onto a body, depends on a multitude of factors such as: shape, material, position, and temperature to list a few. Without an ideal setup the complexities of understanding the magnetic forces behavior on a body is perhaps impossible to generalize. Therefore, it is important to understand the more general cases before. There is a force exerted on a charged particle q, while moving with a velocity v, through an electric field E and magnetic field *B* was first described in an equation by a Dutch physicist (Hendrik A. Lorentz) commonly known as the Lorentz force equation

$$\mathrm{F} = \mathrm{qE} + \mathrm{qv} \times \mathrm{B} \qquad [3]$$

where the magnetic force is proportional to $q$and to the magnitude of the vector cross product $v \times B$. In terms of the angle between this cross product, the magnitude of the force equals $qvBsin\theta$. An interesting result of the Lorentz force is the motion of a charged particle in a uniform magnetic field. If $v$is perpendicular to B($\theta = 90^\circ$), the particle will follow a circular trajectory with a radius of $r = \frac{mv}{qB}$. However, if $\theta < 90^\circ$, the particle will orbit in a helix formation where its axis is parallel to the field lines. Finally, if $\theta = 0$, then there will be no magnetic force on the particle (22).

However, the Lorentz force equation simply describes the forces acting on a single particle, yet when trying to understand the forces acting on a body expressing the equation in terms of area deems more useful towards real world applications. With a few adjustments, the magnetic force for a charge distribution with respect to its area is described as

$$F = \frac{B^2 A}{2\mu_0} \qquad [4]$$

where F is the force per unit area, B is the magnetic flux density, A is area, and $\mu_0$is the permeability of free space. In understanding these mathematical equations, and its physical importance, the use of this on real world applications is possible. A few applications using the Lorentz forces are cyclotron/particle accelerators which allows us to produce x-rays for imaging, cathode ray tubes which allows us to deviate the trajectory of electrons, and bubble chambers allowing us to detect charged particles moving through a medium (23). Although these equations provide a fundamental understanding of magnetism, they are simply a definition for the classical model. Therefore, for a more comprehensive understanding of magnetism, quantum mechanics must be included.

2.1.2 Quantum Mechanics of Magnetism

In the Stern-Gerlach experiment (1922), when exposed to an inhomogeneous magnetic field, it was observed that electrons carry an intrinsic angular momentum known as magnetic dipole moment or “spin”. From this groundbreaking discovery it was deduced that there are only two spin states of an electron, spin ½ “up” or spin -½ “down”. These ½ integer attributes represent the spin quantum number for a certain family of particles (e.g. bosons, protons, and electrons) known as fermions. Fermions obey a very particular law called the Pauli exclusion principle; which states that there cannot be two identical fermions simultaneously being in the same state (position, velocity, or spin). Therefore, if multiple fermions occupy the same spatial probability distribution, then at least one property, such as spin, must be unique. Fermions, in

combination with the Pauli exclusion principle, give us a better comprehension on the origins of magnetic dipoles and will also play an important role in understanding the behaviors of magnetic materials. The quantum mechanical effects of magnetism are much more complicated than what has been simply described here, however, for the purpose of this work this information will suffice.

2.2 Magnetic Materials

2.2.1 Magnetic Dipole Moment

Atomic nuclei are the building blocks of all materials. Electrons, which carry a negative electric charge, orbit the atomic nuclei with an angular momentum as well with the quantum mechanical effect of either a spin up or down intrinsic angular momentum. As mentioned before the motion of a charged particle will create a magnetic field. Therefore, magnetism can be found to some degree in all materials. However, certain materials are more magnetic than others (e.g. iron, nickel, or cobalt). The magnetic strength or dipole moment of a material is governed in part by the configuration of the electrons orbiting the atoms within a material. The magnetic moment of an electron is defined by (2)

$$\mathbf{m}_{\mathrm{S}} = -\frac{g_S \mu_{\mathrm{B}} \mathbf{S}}{\hbar} \qquad [5]$$

Where $\mu_B$is the Bohr magneton, **S** is the electron spin, $h$is Planck's constant, and $g_s$according to Dirac's theory is the g-factor which is a dimensionless quantity that characterizes magnetic moment and angular momentum of a particle.

Atoms with unpaired electrons will experience a net magnetic dipole moment and are considered as atomic magnets, while paired electrons will cancel out to a net zero dipole

moment. For example, iron, which has the most striking magnetic properties, has four unpaired electrons. However, magnetism is not simply dictated by a function of unpaired electrons. This is most evident in pure manganese. Manganese has five unpaired electrons yet has worse magnetic properties naturally than Fe. The reason for this is since the distances between atoms is so small that their moments have a lower energy when pointing in the opposite direction, hence cancelling to a net zero dipole moment. Only when manganese is mixed with other metals, to increase the distance of the moments, will the magnetic properties be enhanced in the form of what are known as Heusler alloys (31). Hence, the complexities of magnetic dipole moments in materials prove detrimental in order to understanding and applying its properties.

Like a compass, this magnetic dipole moment will align in the direction of an applied external magnetic field (H), which will be further discussed in the following chapter. Therefore, a magnetic dipole moment in a magnetic field will possess potential energy dependent on its orientation with respect to the direction of the magnetic field. The potential energy of a magnet with magnetic moment **m** exposed to a magnetic field **B** is defined as the mechanical work of the magnetic force (torque) on the realignment of the magnetic dipole moment vector.

$$\mathrm{E_{p,m}} = -\mathrm{m} \cdot \mathrm{B} \qquad [6]$$

Energy is also stored in a magnetic field, where the energy per unit volume in a region of space known as magnetic permeability μ_0.

2.2.2 Permeability

Not all magnetic materials respond equally to an applied magnetic field (H). Varying materials will exhibit varying flux densities when subjected to the same magnetization amount. To account for such behavior, scientists coined a term to describe the mathematical ratio of flux density to magnetizing force: permeability (μ_0). Permeability, or simply known as the sensitivity of the material, is the ratio of B to H. Every magnetic material has a permeability that is

numerically greater than the value of the permeability of free space - which in CGS units is 1 (27). However, when looking at a hysteresis curve (explained further in the following sections), there are several different definitions for permeability depending where on the hysteresis loop it's referred to.

Thus far, the origins of magnetic materials have been established, which included magnetic dipoles, potential energy, and permeability. Since these fundamental bases have been established, material characteristics where the magnetic dipoles are approximated as independent and non-interacting with each other can be further understood.

2.2.3 Magnetic & Thermal Material Characteristics

For reiteration, not every material will respond similarly under the influence of H. The magnetic susceptibility (χ), yet another intrinsic property of magnetic materials, is a measure of how much a material will become magnetized due to H. The key distinction between magnetic susceptibility and magnetic permeability is that permeability describes the ability of a material to bear the formation of a magnetic field inside itself, whereas susceptibility describes whether a material is attracted to a magnetic field or repelled (25). Mathematically, it is the ratio of magnetization M(magnetic moment per unit volume) to the applied magnetizing field intensity H, seen in Equation 4.

$$\mathrm{M} = \chi \cdot \mathrm{H} \qquad [7]$$

The susceptibility value will signify the exact class of material it represents. There are two basic behaviors a material will react towards an applied H, a.) either an alignment with the direction of the magnetic field, χ>0, called **paramagnetism**, or b.) an alignment against the field, χ<0, called **diamagnetism**. In diamagnetic materials the material will repel the applied field due to an induced magnetic field in the opposite direction, causing a repulsive force. In contrast,

paramagnetic materials are attracted to the magnetic field, caused by the previously mentioned origins such as unpaired electrons, giving rise to measurable magnetic properties within the material. It is important to note however, that an external applied field is not the sole variable to affect the magnetic characteristics of a material: but so is temperature.

All magnetic materials are paramagnetic materials at sufficiently high enough temperatures, this is known as the Curie temperature (T_c), where the thermal energy exceeds the interaction energy between spins on neighboring atoms (1). However, below a critical temperature for certain magnetic materials, spins are observed to adopt different arrays of ordered arrangements. These arrangements consist of ferromagnetism, ferrimagnetism, and antiferromagnetism. Each class is determined by the exchange forces between spins and domain walls. This thesis will briefly go over the definitions of ferri- and antiferromagnetism but focus heavily on ferromagnetism, which is most relevant for the present experimental work. As a quick reference before further explanation for each classification, Figure (1) will illustrate the differences between ferro-, antiferro-, ferri-, and paramagnetic materials in terms of their spin orientation.

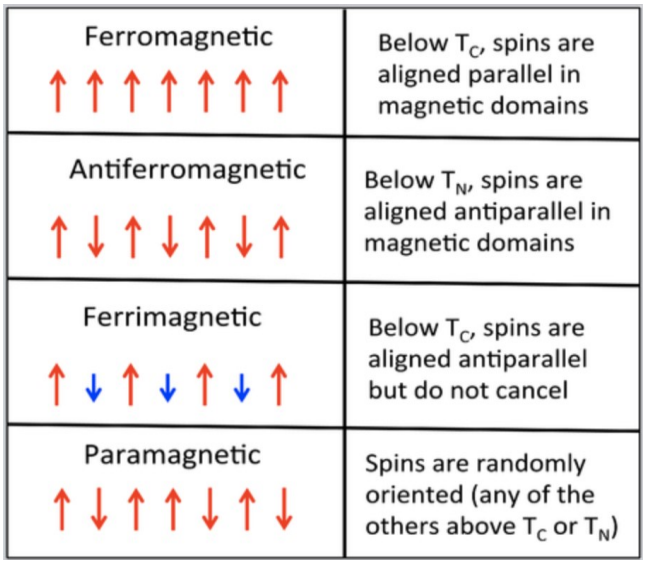

Figure 1: description of the ordering of spins in ferro-, antiferro-, ferri-, and paramagnetism where T_c is the Curie temperature and T_N is the Néel temperature (1)

2.2.4 Antiferromagnetism

Materials in which adjacent ions spontaneously align themselves into opposite, or antiparallel, arrangements throughout the material so that there is almost no gross magnetism produced are known as antiferromagnetic (AF). This orientation of spins is intrinsic to the material and observed even in the absence of an applied field. Some materials that exhibit AF behaviors include certain metals, alloys, in addition to some ionic solids. As previously mentioned, the magnetism from the dipole moments of the atoms aligned in one direction is canceled out by the set of neighboring dipole moments of the atoms aligned in the opposing direction (Fig. 3). AF solids exhibit special behaviors depending on temperature. They are distinguished from other materials in that their susceptibility value (χ) increases as temperature rises, whereas χ decreases in value as temperature rises for paramagnetic materials (4). At a critical temperature, called the Néel temperature (T_N), which is analogous to the Curie temperature (T_c), there is a disruption to the antiparallel coupling due to high thermal fluctuations. If antiparallel coupling is lost, the material will then be susceptible to a change of magnetic domain direction under an applied field. While below T_N, the AF solid will exhibit no response to the external magnetic field due to the rigidity of the antiparallel ordering of the dipole moments. At higher temperatures, but still below T_N, some magnetic moments will break free and align with the field. This alignment will produce a weak but measurable magnetism within the material. However, above T_N thermal agitation will progressively prevent alignment of the atoms with the magnetic field, so that the magnetism produced in the solid by the alignment of its atoms continuously decreases as temperature is increased (4).

2.2.5 Ferrimagnetism

Ferrimagnetic materials are like AF material in that their atomic dipole moments are antiparallel. Yet, the magnetic moments strength between neighboring dipole moments are "unequal" (Fig. 3). Ferrimagnetism is a term that was originally coined by Louis Néel (a prestigious French physicist and also the discoverer of the Néel temperature in antiferromagnetic materials) to describe the magnetic phenomena in ferrites, in which Fe ions appear in two different ionic

states and hence bear different magnetic moments with mutual antiferromagnetic coupling (9). In result, due to this unequal exchange of moments, there exists a net magnetization. Similarly, ferrimagnetic materials exhibit the same hallmark properties as does ferromagnetism (discussed in the following chapter) such as: spontaneous magnetization, Curie temperatures, hysteresis, and remanence. The major outlier once again, are its magnetic ordering. Ferrimagnetic ordering is most common in metal oxide materials (such as Fe^{2+} and Fe^{3+}). Ferrimagnetic materials have anisotropic properties and high electrical resistivity. Like most materials, ferrimagnetic properties are susceptible to change under the influence of both thermal and magnetic externalities.

2.2.6 Ferromagnetism

In ferromagnetic materials, the alignment of electron spins is parallel (Fig.3). This alignment results in a large localized net magnetization, which means that the material produces a magnetic field even in the absence of an external magnetic field. The alignment of the spins or magnetic moments are confined within tiny asymmetrical regions of the bulk material called magnetic domains. Within each domain the spins or magnetic moments are aligned as mentioned before, however, the magnetic moments within neighboring domain walls are not necessarily oriented in the same direction. This concept is clearly illustrated in Figure 2.

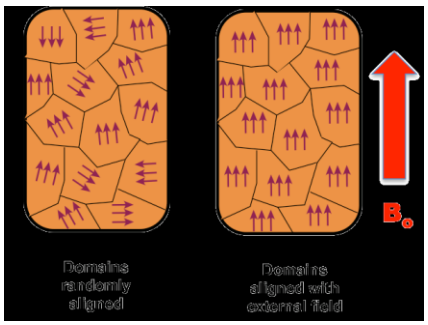

Figure 2: Dipole moments oriented randomly between domains (left), dipole moments aligned due to external field (right) (12)

The random orientation of domain walls is because the exchange interaction of electrons is a short-range force. In fact, the short-range exchange forces between the electrons are so large they are equivalent to a field on the order of 1000 Tesla, or approximately a hundred million times the strength of the earth's field (9)**.** However, over long distances, to minimize energy, certain domains will orient themselves in a varying direction to their neighbors. Consequently, when in its lowest energy state, the bulk material will generally have little to no net magnetic field. Since the magnetic moments of the domain walls are not fixed, they are susceptible to change when exposed to an applied magnetic field.

For ferromagnetic materials, if an external magnetic field is applied to the bulk material the magnetic moments within the domain walls will align parallel to the direction of the applied field (Figure 2). This occurs in part due to the magnetic moments experiencing a torque exerted by the field.

$$\vec{\tau} = \vec{\mu} \times \vec{B} = \gamma \vec{J} \times \vec{B}, \quad [8]$$

Where τ is the torque, μ is the magnetic dipole moment, J is the angular momentum vector, B is the external magnetic field and γ is the gyromagnetic ratio which is equal to the ratio of the charge of the particle, a unit-less proportionality factor relating the system's angular momentum to the intrinsic magnetic moment, and its mass. Yet, the magnetic moments will not directly align with the field straightaway, but instead precess around the unidirectional axis of the magnetic field vector. This is known as the Larmor precession. This phenomenon is like the precession of a tilted gyroscope in classical dynamics. The rate at which the precession of the magnetic moment occurs about the field axis is known as the Larmor frequency.

$$\omega = -\gamma B \quad [9]$$

Where ω is the angular frequency, B is the magnitude of the applied magnetic field, and γ is once more the gyromagnetic ratio. As you can see from the Larmor frequency equation, the rate of precession is dependent on the direction of the magnetic field to the system and the amount of energy required to change orientation.

Due to the random distribution of directional magnetization in the domains of ferromagnetic materials, there exists magneto-crystalline anisotropy. This means that for a domain there will be an easy axis along which it prefers to be magnetized (i.e. magnetization in this direction gives an energy minimum for the domain). If the direction of an applied field differs from the direction of the easy axis, extra energy will be required to overcome its barrier (22). The energy required to rotate the magnetization from its easy axis is different for different materials and described with this Equation (11)

$$E_{an} = K sin^2 \phi \qquad [10]$$

Where E is the energy required, K is a magnetic anisotropy constant specific to the material, and ϕ is the magnetization angle from the easy axis. Larmor precession will occur when, $\phi \neq 0$. It is important to note that the ease at which the domain walls are susceptible to change is not only due to the direction of the applied field and energy but is also reliant on the homogeneity and micro-structure (e.g. grain boundaries, inclusion, or dislocations) within the material. This varies greatly with all ferromagnetic materials.

Saturation and Hysteresis

When there is enough input energy in the system, there will be a moment where the maximum alignment of magnetic moments of the domain walls is reached. This point is known as saturation. The saturation point of magnetization is the maximum induced magnetic moment, in a certain direction, that can be obtained within a material. No matter how much applied field you exert onto a ferromagnetic material after saturation, the magnetization will stay the same.

This behavior can be visualized for a ferromagnetic material when measuring the magnetic flux density as a function of the applied field, or more simply known as the B-H curve. For example, in Figure 3 we see the B-H curve for ferromagnetic material: magnetite.

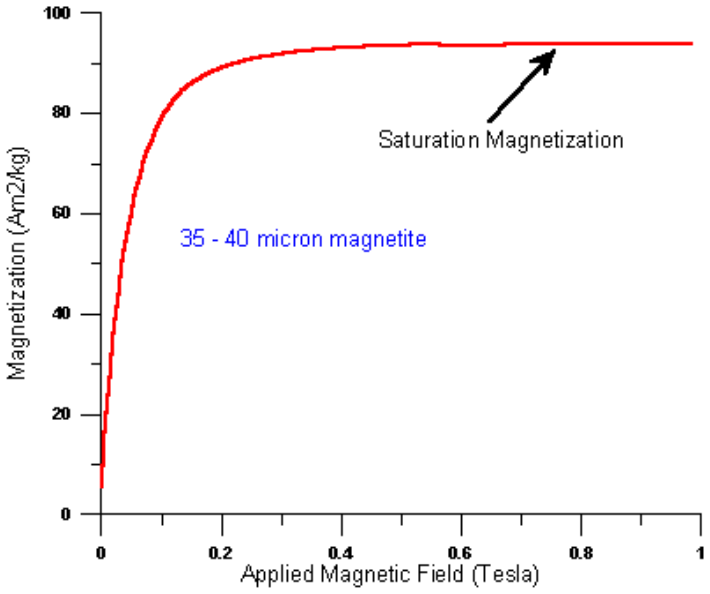

Figure 3: B-H curve of magnetite (9)

When enough field strength is applied to the material (in this case 0.2 T) there becomes a point in the curve where it plateaus. This plateau represents the point of saturation. When saturated, even when the external field is removed for certain ferromagnets the material will stay magnetized, and in order to demagnetize it requires enough heat or simply a magnetic field in the opposite direction of the magnetic dipole moments. However, there is a phenomenon that occurs when demagnetizing the material, in that it will not follow the same curve back as it had done originally.

Hysteresis is the dependence of the magnetic state of a system and on its history. Once magnetized in one direction, it will not follow the same path back when a field is applied in the opposite direction. In fact, when an alternating magnetic field is applied, the magnetization will

trace out what is called a hysteresis loop. In Figure 4, is a depiction of a typical hysteresis loop curve.

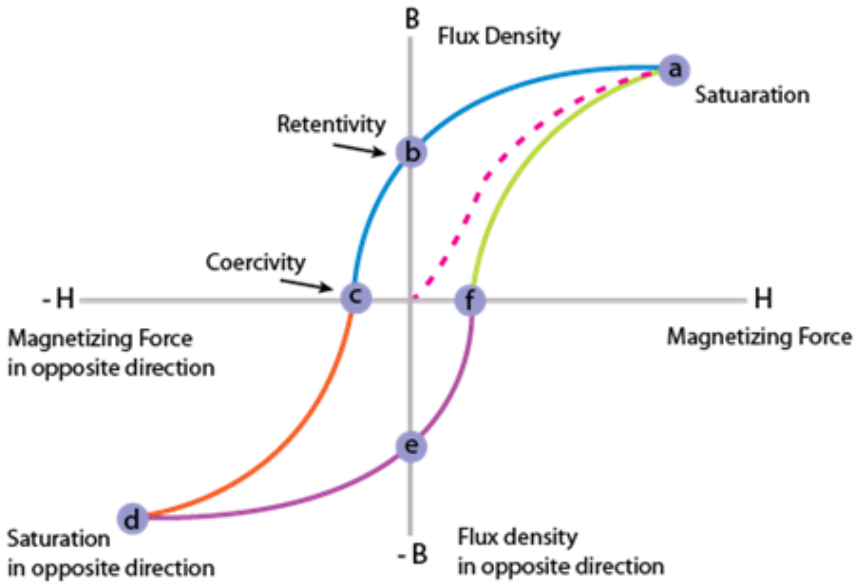

Figure 4: B-H curve depicting a full hysteresis with a description of key points (8)

The hysteresis loop contains critical information on the magnetic properties of a material. One of the most important details of the curve is coercivity or coercive force (H_c). Coercivity represents the amount of opposing field strength that is required to demagnetize a material. If a little amount of field is required to demagnetize, then the material will have a low coercivity value. In contrast, if there require very strong fields to realign the domain walls, then the material has a high coercivity. Materials with low coercivity are considered as “soft” magnets while high coercivity materials are “hard” magnets. Figure 5 illustrates the differences between soft and hard magnets in a B-H curve.

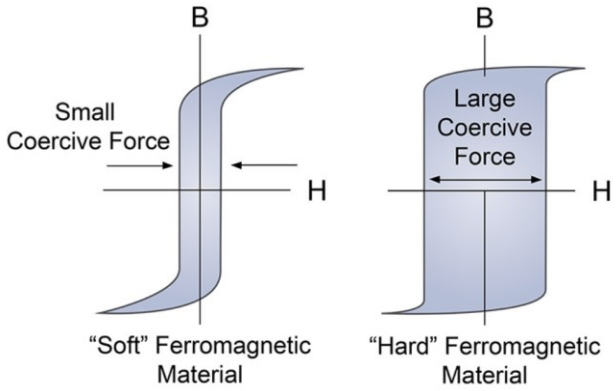

Figure 5: A comparison of hysteresis showing the difference between soft magnets (left) and hard magnets (right) (41)

As is evident from this figure, the width of the B-H curve can be a major indicator of whether the ferromagnetic material is a soft or hard magnet. Soft magnetic materials (SMM) are widely used in our everyday lives and are an important topic revolving around this thesis.

2.3 Soft Magnetic Materials

In 2018 the global electricity consumption reached a staggering 157,063.77 TWh (35). This is a 663% increase from 2015 where the global consumption was 20,567 TWh. At this rate of continuous growth of consumption, we are in high need for further innovative technology associated with clean energy supply at an affordable cost. Hence, there exists a pursuit towards research and the development of energy-efficient materials. One potential solution for this demand revolves around soft magnetic materials (SMM). SMM currently occupies a prominent economic position as an indispensable component of all modern devices that include consumer goods (e.g., laptops/smart phones), hybrid vehicles and data transmission systems. Presently, according to the Consumer Technology Association (CTA), "cutting-edge" technology contributed a staggering 377 billion USD to the entire consumer industry (28). This value is sure to exponentially increase with future implementations of 5G network, smart homes, quantum computing, and artificial intelligence (AI). Furthermore, SMM are also crucial towards the energy

industry. To meet the increasing demand, SMM have been implemented as components to already existing technologies in providing/storing energy more efficiently, cost-effectively, and sustainably. An example of this can be seen within flywheel technology. Thanks to SMM flywheels have become more feasible and, in many respects, a better solution to chemical energy storage devices such as lithium-ion batteries, where a typical lithium-ion battery has a life-time of 3,000 charge and discharge cycles while flywheels can have over tens of thousands (6). Certain subclasses of SMM incorporated within flywheels allow higher magnetic flux densities at higher frequencies, improving overall performance. Although SMM have greatly enhanced the potential of new and existing devices, they still face many challenges and limitations towards global implementation. It is necessary to note that there are many subclasses of SMM, and for the scope of this paper it will revolve around the subclass known as *soft magnetic composites* (SMC).

2.4 Soft Magnetic Composite

2.4.1 Introduction

SMCs comprise of ferromagnetic materials in combination with an electrically insulating binder, which is generally produced using the powder-metallurgical techniques of compaction and heat-treatment. The term “soft” in SMCs, as previously described, depicts the materials susceptibility to demagnetization under the influence of a “weak” external magnetic field as a function of the coercive field H_C. This unique property has many advantages for a wide array of applications, which will be further discussed in the following chapters. Some of the main advantageous properties inherent to SMC are their isotropic magnetic nature, low eddy current loss from high electrical resistivity, reduction in size and weight, and the possibility to create complicated 3D magnetic shapes (5). In terms of physical requirements SMCs are expected to exhibit minimal energy loss in combination with low magnetostriction (variation of physical dimension when a magnetic field is present in the environment), high saturation polarization J_s (related to the orientation of magnetic moments per unit volume of the magnetic material), and largest possible permeability (μ_0) (5). A distinct characterization of the magnetic properties in

SMC comes from its μ_0. The permeability, a closely related property to susceptibility (χ), directly links both the magnetic field strength **H** and flux density **B** with the equation:

$$B = (\mu_0)(\mu_r)H \quad [11]$$

where in this case (μ_0) corresponds to the magnetic permeability of free space ($4\pi \cdot 10^{-7} N \cdot A^{-2}$) and μ_r refers to the relative permeability.

When it comes to permeability of SMC materials, some typical values of maximum permeability are (37):

- Molly Permalloy Powder = 14 to 350 H/m depending on powder loading
- Powdered iron = 8-75 H/m
- Silectron = up to 30,000 H/m
- Supermalloy = up to 300,000

Unfortunately, the permeability of magnetic materials is not constant, especially for SMC. As the excitation (applied field) varies the permeability will decrease at a rate linked to the frequency and strength of the excitation. In addition, permeability is affected by their environment caused by temperature and mechanical shock. Therefore, it is necessary to keep this in mind when making material selection for one's desired applications. In the following sections, the topics ranging from material selection to application of SMC will be discussed in further detail.

2.4.2 Material Selection

Powder Cores

When it comes to the selection of materials in SMC applications, the ferromagnetic family (e.g. Fe, Co, and Ni) along with soft ferrites (i.e. ceramic compounds based on iron oxides in addition with other metallic elements), are the major options for SMC production due to their

natural ferromagnetic properties. In the interest of this thesis, Fe will be the reference element material henceforth. For certain SMC applications, the ferromagnetic materials have been realized by stacks of laminated magnetic sheets. This approach has been limited in terms of the magnetic design being confined to a 2D approach. However, thanks to the development of powder metallurgy, it is now possible to increase the magnetic performance through a 3D design.

For powders, the purity, shape, and size of the particles will all have a major influence on the magnetic and mechanical response to the system. Smaller size particles result in finer powder, which leads to composites with constant permeability/frequency characteristics and lower loss at high frequency compared to coarser powders (30). However, coarser powders generally present higher permeability. This is a plausible conclusion since the permeability relation is linked between flux density and magnetic field strengths, which was previously understood. In fact, the effects of magnetic permeability dependence on particle size has been extensively researched for a few decades now. Higher permeability of the magnetic loaded composite is commonly attributed to larger particle size (30). An equation has been derived by Polyakov and Egorov, which shows the relative permeability increasing with the square root of the particle size for a porous ferromagnetic body in the form:

$$\frac{\mu}{\mu_r} = (1 - P)\left[1 - K' + K'\left(\frac{D}{D+AP}\right)^{\frac{1}{2}}\right] \quad [12]$$

Where *P* refers to the porosity of the SMC, *K'* is a coefficient representing the fraction of the structure-sensitive contribution to μ_r, *A* is a coefficient independent of P, and D is the particle size. Although powdered form has proven to be versatile for application, a recent class of fiber-based SMC has been studied and proven to improve magnetic properties compared to powder form.

In 2019, what is considered as the first report on a new class of SMC deemed “fiber-based soft magnetic composite (FSMC)”, was prepared using long iron fibers instead of ferromagnetic

particles and coated with a polymeric layer. Both AC and DC magnetic properties were investigated with respect to the influence of polymer content and material preparation. It was found that both compaction pressure and polymer content play an important role in the magnetic properties. The FSMC studied presented superior AC and DC magnetic properties when compared to a powder-based SMC prepared in identical conditions (43). Although the magnetic properties of FSMC deemed superior, compared to powder SMC, it has yet to be verified whether its mechanical properties have similar enhancements. Regardless, with this study, fiber-based SMC could potentially become a viable solution for future SMC applications.

Organic Based Insulating Coating

The insulating coating that separates the individual iron particles in an SMC product is the paramount feature of this technology. It serves as a dual purpose by both increasing bulk electrical resistivity and mechanical properties. Everything from viscosity, coverage, thickness, and endurance in combination with the processing procedure are key aspects towards both mechanical and magnetic properties of the composite. These coatings, in general, can be divided between two large families known as organic or inorganic based resins.

When it comes to organic based resins there are two types; thermoset and thermoplastic resin. The physical difference is that thermoplastics can be re-melted into a liquid, whereas thermoset resins are irreversible from permanent solid state. Thermoset plastics contain polymers that cross-link together, normally after the addition of an agent, during the curing process to form an irreversible chemical bond, while the cross-linked bonds for thermoplastics are more flexible. A benefit of thermoplastics and its reversibility characteristic is that it allows thermoplastics to be remolded and recycled without having a negative effect on the material's physical properties (21). This allows a sustainable means to reusing any byproducts of production. Overall, organic resins tend to be the preferred option for SMC production since they act as binder media and introduce acceptable mechanical strength to the overall part.

Inorganic polymers offer properties not found in organic materials including electrical conductivity, nonflammability, and low-temperature flexibility (40). The term “inorganic” polymer generally refers to one-dimensional polymers rather than the heavily cross-linked polymer chains found in organic based compounds. Consequently, for these unique properties, electrical insulations based on inorganic compounds allow for high temperature heat treatments that may yield better magnetic properties. However, a key property required for SMC application are its mechanical properties, which is why organic based resins are more popular. Yet, organic based resins are not without its flaws.

There are drawbacks to using organic based resins. They for one cannot be used in too large of volume due to the reduction in permeability that they naturally impose. Another negative aspect is that they are limited in thermal stability (especially thermosetting resins). On the other hand, thermoplastic resins offer improved stability, but have worse surface coverage of the powder particles (21). However, these negative properties do not hinder the positive benefits it has towards the mechanical properties. Therefore, when it comes to deciding the choices are between thermoset or thermoplastic. This choice all depends on the intended application. The current work of this thesis, thermoset based resins will be utilized. Therefore, it is relevant that the topic be understood a bit further.

Some of the most common and widely used organic thermoset resin includes: Polyester Resin, Vinyl Ester Resin, Epoxy, Phenolic and Urethane. Thermosets tend to be the preferred choice for SMC because when uncured they are in liquid form, which allows for convenient impregnation of reinforcing the iron particles or fibers. As a liquid in room-temperature, thermoset resins are straightforward and easy to work with. Although it requires adequate ventilation for open-air production applications, for closed molds manufacturing the thermoset can be shaped quickly using a vacuum or positive pressure pump, allowing for mass production of superior products at a low raw-material cost (21). The biggest drawback of thermosets, once again, is their irreversibility. As a cause for this, recycling thermoset products have become an increasingly relevant concern for SMC mass production. However, the negative outcomes for

using thermosets does not outweigh the substantial benefit it has towards the mechanical properties of SMC, which is why thermosets tend to be chosen over thermoplastics.

2.4.3 Classification/Processing

Introduction

SMCs are typically produced using powder metallurgy techniques (e.g., compaction, heat treatment, curing, and annealing procedures). When preparing, one generally applies a bonding agent, thermosets for our purposes, to the ferromagnetic powder before heat treatment. Most common methods for applying such surface layers on powder materials are either immersion baths, sol-gel methods or through oxidation during annealing (29). This will encapsulate the individual particles in 3D structures as represented in Fig 6.

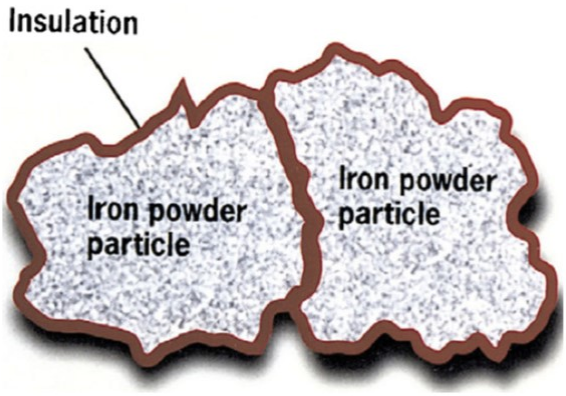

Figure 6: Individual particles (in this case Fe) layered with electrically insulating bonding agent (35)

Some major advantages of this technique are low core losses at a higher frequency, both cost effective with an emphasis in sustainability, and unlike laminate steels, incorporate 3D flux capabilities. In addition, extremely sophisticated components with a higher degree of complexity can be met through production of SMCs as seen in Figure 7.

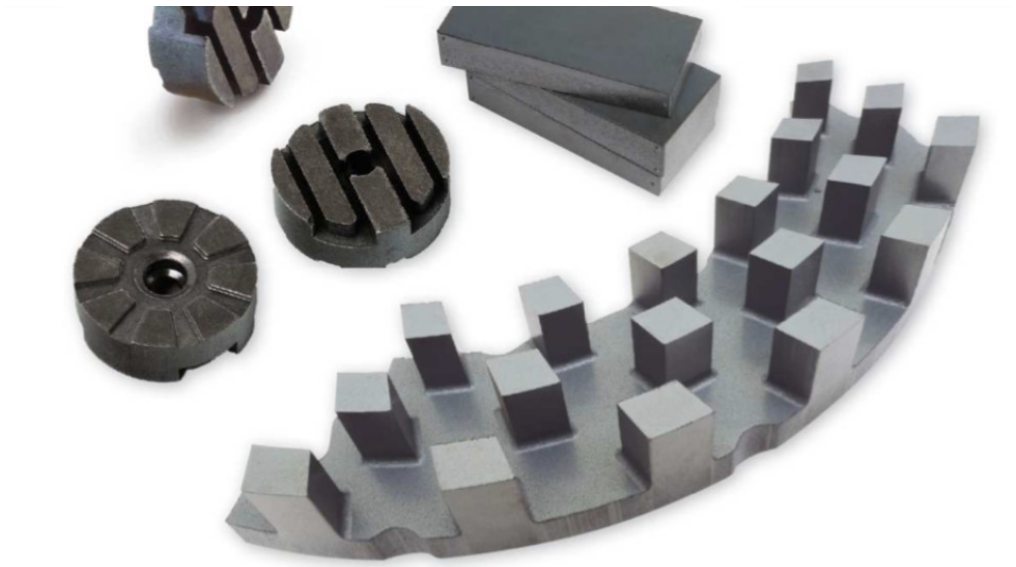

Figure 7: Complex SMC components for electric applications (5)

Compaction

One of the initial procedures when assuring quality production of SMC is with the compaction process. There are a wide range of techniques used: from manually compressing to high powered machines which can achieve extremely high pressures. However, one must be aware and careful that under extreme pressure, the insulating layers can be destroyed. Destroyed in the sense that the soft-magnetic particles should not encounter each other. If adjacent particles would connect directly with each other, then the eddy-current loss (further elaborated in Section 2.1.4 Applications) would increase sharply as a result (29). On the other hand, pores can be found if pressures are not high enough. Pores would act as dislocations that impair magnetic and mechanical performance. Studies have shown that a type of phosphorus-added iron-based alloy under the pressure of 400-800 MPa at room temperature with the highest density, yielded the highest maximum permeability but the particle deformation caused a large coercive field (29). Therefore, one can imagine the intricacies of the compaction process and how important it is on the SMCs overall properties.

Heat treatment

Heat treatment is an indispensable process in SMC preparation as a way to reduce internal stresses. However, insulating binders can decompose into carbon at sufficiently high enough temperatures. Therefore, it is important to understand the various techniques used for the enhancement of SMC. Heat treatment can occur throughout a wide range of temperatures, however, when temperatures are high enough it is then considered as “annealing”. Annealing can benefit SMC production for example a more homogenous distribution of binding contact layer to particle surface. However, the ideal temperature will be highly dependent on factors such as: glass transition of resin, thermal properties of particles, and mixing ratio. The effects of heat treatment on the magnetic properties of iron-based SMC were investigated, showing that as temperatures increase (upwards to 873K), the lubricant gradually decomposes. The leaving decomposition product reacted with the iron oxides, which made the frequency stability of the permeability decrease especially at high frequencies. In addition, the resistivity decreased significantly, and the eddy current loss increased as well (10). Therefore, the heat treatment process adds another layer to the already complex process of producing effective SMC. Above all, a suitable combination between the compaction process and adequate annealing process would have a great contribution towards the soft magnetic properties of the SMC.

2.4.4 Applications

Alternating vs. Direct Current Applications of SMC

There is a wide use of SMC applications, which depend on a myriad of factors entailing material selection, combination, and processing techniques. For certain processes will yield certain properties that in turn will suit some applications more than others. However, when it comes to SMC applications there are generally two main categories: direct current (DC) and alternating current (AC) applications.

For DC applications the material is magnetized during the operation, in order to perform its task, then demagnetized at the conclusion of the operation (e.g. a magnetic crane). A major SMC DC application is about magnetic shielding. Magnetic shielding is where a high permeability magnetic material is used to encapsulate the device which requires shielding (26). Most permanent magnets used in devices such as MRI body scanners, use SMC in combination with DC applications as well. Therefore, properties required for DC applications entail high permeability and high coercivity.

In AC applications the SMC material will continuously change magnetic state directions throughout the period of operation. This type of application is very common within power supply transformers, which is found in computers, electric vehicles, aircrafts, and medical devices. Therefore, for AC application a high permeability, low coercive field, and low hysteresis loss are required (35). The requirements for both AC and DC applications, in terms of their B-H curve, can be better visualized in Figure 8. The requirements for DC applications are not specifically described within Figure 8 however, the hysteresis with a larger coercivity would be ideal for DC applications.

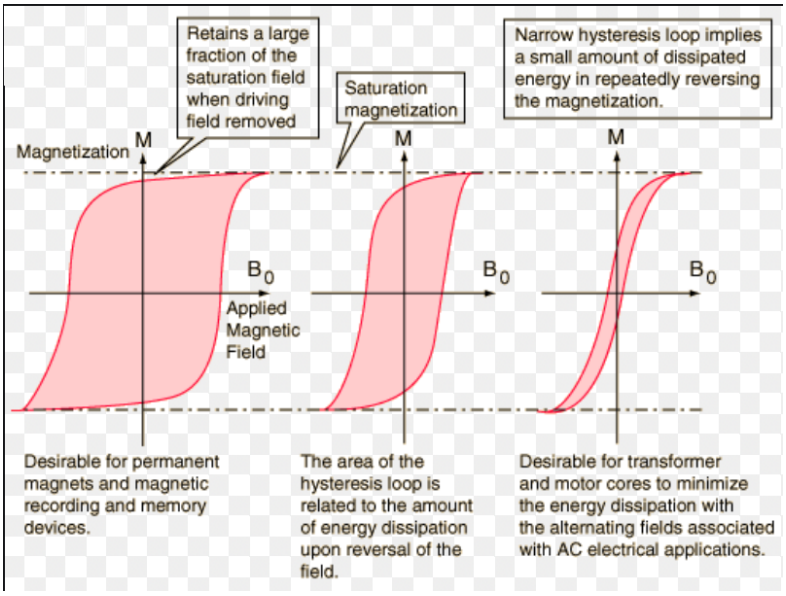

Figure 8: Variations in hysteresis of different materials and their respective applications (16)

There arises, however, complications with SMC when it comes to AC applications. A consequence, from applying a varying field, is the diminution of energy within the system as the material is cycled around its hysteresis loop. This loss is known as core losses and is due to resistance occurring within the material. Core losses can be subdivided into three parts:

1. Hysteresis loss (P_h)
2. Eddy Current loss (P_e)
3. Residual loss (P_r)

Hysteresis loss originates from the irreversible magnetization process existing within the magnetic material (i.e. the irreversible displacement of the domain wall and irreversible dynamic behavior of the magnetic domains) (26). This will cause a reduction of the intrinsic coercivity property of the material, which is related to the area contained within the hysteresis loop (Fig. 13). Hysteresis loss can be expressed by:

$$P_h = f \oint \quad H \cdot dB \qquad [13]$$

where $P_h$is the hysteresis loss, $f$is the frequency, H is the magnetic field strength and $B$is the magnetic flux density. For iron powder materials, the factors that lead to hysteresis losses are caused by impurities (i.e. distortion between inter-particle grain boundaries). Therefore, to reduce any hysteresis losses, the purity of the material must be high. In order to increase purity, and improve the stressed regions, various heat treatment/compaction techniques must be implemented during preparation.

Eddy current losses are a result of electromagnetic induction (electrical resistance losses) in the material caused by an alternating electric field. When eddy currents are induced in

materials, two main effects are observed: incomplete magnetization of the material (skin effect) and increase in core losses (34). Eddy current loss can be expressed by:

$$P_e = \frac{CB^2 f^2 d^2}{\rho} \quad [14]$$

where P_e is the eddy current loss, $C$is the proportionality constant, $B$is the flux density, f is the frequency, $\rho$is the resistivity and d is the thickness of the material. In order to limit any eddy current losses, certain techniques are used which include adding silicon (Si) to the iron powder, using thinner laminates, or coat with an inorganic coating at high temperatures (34).

Although hysteresis and eddy current losses make up most of the core losses, there are still certain unrelated losses found within the system. Residual loss includes all other losses apart from eddy and hysteresis losses. The origins of residual losses are still not fully understood but are known to be caused by the magnetic relaxation processes. Residual loss is mainly magnetic after effect loss, in a low-frequency and weak magnetic field scenario, therefore, will have nothing to do with the frequency. However, high frequency residual losses include losses caused by size resonance, domain wall resonance, and natural resonance (26). The residual losses can either be caused by the induced anisotropy generated by once again impurities, caused by thermal fluctuations, or even due to the proliferation of valence electrons between the ions.

2.5 Challenges/Future of SMC

Despite SMCs great advantages in electrical/magnetic properties, it is countered by certain disadvantages. Their production at larger scale is greatly hindered due to various lack of performance such as high hysteresis loss resulting from stresses induced by the compaction processes, low magnetic permeability/induction caused from low density and sequential air gaps, difficulty to properly insulate individual particles with bonding agent (a major cause for large scale eddy current losses), and finally poor mechanical properties. Therefore, proper material selection and process treatment are hence very important aspects that can further promote

overall performance. Part of the objective of this thesis will be to understand and perhaps discover novel means of optimizing the magnetic properties of SMC. Before these issues are solved, an adoption towards a large market will simply not be possible.

3. Experimental

3.1 Materials

3.1.1 Soft-Magnetic Powder

The soft-magnetic material used for every experiment was carbonyl iron powder, with an average particle size of 5-9 μm. It was purchased from Sigma-Aldrich (20). It has a dark grey color and very fine quality.

3.1.2 Resin

Three different resins were used for the experiments.

Table 1: Thermoset resins used for experiments

Resin	Hardener	Mixing ratio: wt%	Mixing ratio: vol%
Sika Biresin CR131	CH135-8	100:21	100:26
G/Flex 650-8A	G/Flex 650-8B	1.2:1	1:1
Biothan 2MD 207E	Biodur M330	100:78	100:83

Sika Biresin CR131 with hardener CH135-8 is an epoxy resin system designed for infusion and injection processes, especially for applications where a higher thermal resistance is needed. It has an optimized viscosity designed for good impregnation and fiber wetting properties. Depending on curing conditions, glass transition temperatures up to *140*˚C can be achieved.

Curing conditions is 8 hours at 140°C, with a tensile strength of 89 MPa, flexural strength of 129 MPa, shore hardness of D86 and a combined density of 1.17 g/cm^3(7).

G/Flex 650 is a toughened, versatile, liquid epoxy for permanent waterproof bonding of fiberglass, ceramics, metals, plastics, damp and difficult to bond woods. With a modulus of elasticity of 1GPa, it is a bit more flexible than standard epoxies and polyester, but much stiffer than adhesive sealants. This gives it the ability to make structural bonds that can absorb the stress of expansion, contraction, shock, and vibration. Reaches an initial cure in 3-4 hours and a workable cure in 7-10 hours at room temperature (38).

Biothan 2 MD 207 E is a casting resin consisting of rapeseed esters, sugars, sunflowers, as well as polyols mixed with various additives. This gives it overall good thermal conductivity and resistance. Its low viscosity of the combined resin with Biodur hardener allows for quick and easy mixing and large quantities of castings (39).

3.2 Methods

3.2.1 Sample Dimensions

It is crucial to choose the correct mold for the curing process before commencing any sample preparation. Since our samples are subject to various mechanical tests, as well as magnetic, it is then recommended to adhere to certain guidelines regarding specimen dimensions. The standard used, which are described in Figure 9 and Table 2 (below), is the EN ISO 527-2 Plastics for determination of tensile properties.

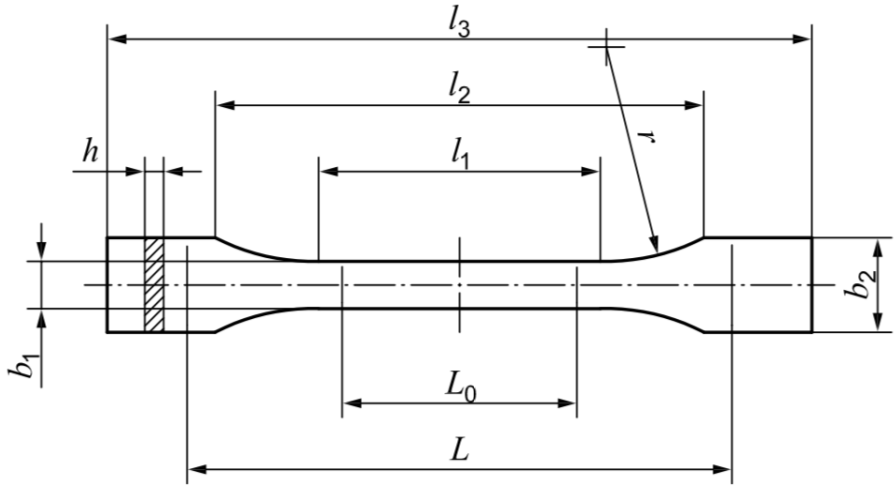

Figure 9: Schematics for specimen dimensions

Table 2: Dimensions for Standard test specimens

	Specimen type	**1BB**
l_3	Overall length	*≥ 30*
l_1	Length of narrow parallel-sided portion	*12.0 ± 0.5*
r	Radius	*≥ 12*
l_2	Distance between broad parallel-sided portions	*23.0 ± 2.0*
b_2	Width at ends	*4.0 ± 2.0*
b_1	Width at narrow portion	*2.0 ± 0.2*
h	Thickness	*≥ 2*
L_0	Gauge length	*10.0 ± 0.2*
L	Initial distance between grips	$l_2 + 1$

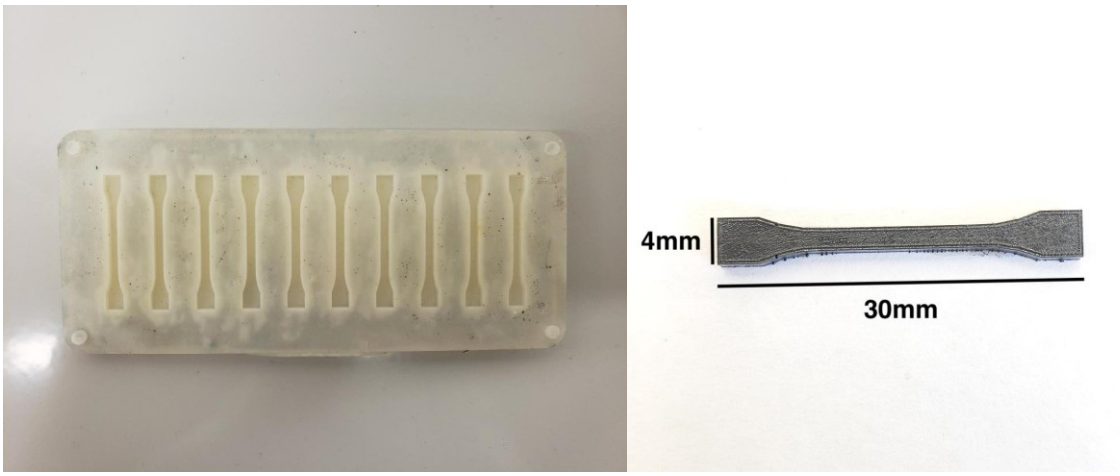

Figure 10: **left**.) Silicone mold with 10 slots of 1BB dimensions; **right**.) Typical outcome of testing samples

Depicted above is the exact mold used with exact 1BB dimensions Figure 10 (left). Figure 10 (right) depicts the general outcome of my samples. The shape is well adhering to the tensile testing dimensions guideline represented in Figure 9.

3.2.2 Sample Preparation

For Biresin CR131/CH135-8, it became a unique two-part experiment which differed in terms of mixing ratios of epoxy to Fe powder. What stayed constant was the resin to hardener mixing ratio which was 100:21 weight percent. However, for the first sample, 50/50 Fe/Resin weight% mixing ratio was used. For the second sample, a mixing ratio of 70/30 Fe/Resin weight % was made. The goal for having two distinct samples, was to further elucidate on the importance of mixing ratio when it comes to the quality of SMC.

Batch 1: The Biresin CR131 was translucent with viscous texture while the CH135-8 hardener was yellow and low in viscosity. With a scale, 30.173 grams of Fe particles, 21.6 grams epoxy, and 8.4 grams of hardener were measured, to attain a mixture with 50 wt% resin system and 50 wt% Fe particles. Initially, the epoxy and hardener were manually mixed for one minute after which, Fe powder was slowly poured into the mix. After several minutes of hand mixing, the liquid substance was poured into the 1BB silicone mold. The mold was then left to harden at room temperature for 12 hours. Afterwards, the mold was placed in an oven for curing at a

temperature of 140 ^{o}C for 8 hours. Following the curing, the samples were left for another 12 hours at room temperature to cool.

Batch 2: Similarly, to batch 1, every step was followed to exact detail except for the quantity used. 35.00 g of Fe powder was mixed with 11.85 g of epoxy and 3.15 g of hardener, targeting a 70/30 wt% mixing ratio.

For G/Flex 650, a mixing ratio had been previously optimized as 70/30 wt% Fe/Resin. The resin was clear in texture while the hardener was clear with a tint of light brown coloring. Resin mixture, containing 9.02 grams of premixed G/Flex epoxy in accordance with the 1.2:1 resin/hardener ratio, was exposed to vacuum for approximately one minute. Afterwards, 21.44 grams of Fe particles were manually mixed with resin for a couple of minutes. The ensuing mixture was then manually placed into the 1BB silicone molds. Molded samples were then cured/heat treated for 24 hours at room temperature, as instructed by the manufacturer. The texture of the samples after this method was much softer than that of CR131. However, the producers of G/Flex have formulated this on purpose. It contains elastomers that make it extremely flexible. Although, his softness and low elasticity could possibly indicate poor mechanical properties.

For Biothan and Biodur/Fe SMC samples, a mixing ratio of 70/30 weight % was used. The resin was a light cream color while the hardener was clear in texture. The Biodur hardener was weighed out to 6.6 grams while 23.4 grams of Biothan was weighed to reach the required 78:100 ratio. For this method, it was advised that the Biothan resin be poured into the hardener and not the other way around, which has been the method I've used for all other resins. The mixture was then kept in a vacuum for at least two minutes before adding Fe powder. Succeeding, 70 grams of Fe powder was slowly poured into the resin mixture until the substance turned into a dark silver paste. The mixture was then poured into the mold and left for 12 hours at room temperature. The following mold was then annealed at 80 ^{o}C for two hours. After the two hours,

the samples were left to cure at room temperature for 36 hours. Similarly, to the G/Flex sample, these samples were very soft. However, it was able to bend much more than that of the G/Flex.

3.2.3 Scanning Electron Microscopy

For the needs of surface morphology characterization, for both powder samples and SMC specimens, a scanning electron microscopy (SEM) was implemented using a Thermo Scientific Phenom Pure Desktop SEM. Its specifications include an electron optical magnification range (80-65,000x), resolution ($\leq$25nm), black & white light optical navigation camera, low-high vacuum mode, and a standard backscattered electron detector. A 5kV was used to capture the images and magnification ranges used varied between 205-20,000x.

For better SEM resolution of surface morphology, a Q150R sputter was utilized. The Q150R is a compact rotary-pumped coating system suitable for SEM sputtering with non-oxidizing (noble) metals - e.g. gold (Au), gold/palladium (Au/Pd) and platinum (Pt). Coating of Au at 20 mA for 30 seconds was used for every sample.

3.2.4 Magnetic Force Sensing

The magnetic force sensor (MFS) is a device entirely constructed by myself for the purpose of measuring the magnetic forces of SMC specimens in units of grams (g), which can be converted to Newtons (N), considering that 1g corresponds to the gravitational force experienced by a 1g object, i.e. 0.00981N. The entire construction is detailed in Appendix (A7.1), which includes step by step processes taken and parts utilized. However, essentially, there are two main components which control the MFS: stepper motor & laser sensor. Software utilized to control Nema 23 stepper motor (32) was a programming language for motion control applications called Trinamic's TMCL-IDE (3.0.25.0). Software utilized to control the optoNCDT laser (18), is the ILD1420 DAQ Tool V3.5.7. This programming language uses triangulation to measure accurately (1μm) distance. Finally, to plot all measurements OriginPro 2020 is a software for interactive data analysis and scientific graphing.

Once the MFS was set up and securely fixed into position, and samples for testing were prepared, necessary connections to run the device were made. Using a Velleman DC switching power supply, both laser and stepper motor were running at 24V. The load cell, which connected to the Arduino uno, was powered by 5V. The Trinamic, Micro-Epsilon, OriginPro, and Arduino code window softwares were all open and connected to their respective devices. Without tampering with the set-up, using the Trinamic stepper motor control software, the lead screw table was adjusted to where the position of the face of the permanent magnet (PM) was flush with the surface of the sample head (Appendix 7.1). This would allow a zeroing of the position signal displayed on the optoNCDT 1420 software. Once zeroed, I would readjust the position of the PM backwards roughly 15mm away from the origin. Shortly after, I would remove the sample head from the load cell and place an SMC sample into its respective slot. Upon making sure that the sample was properly placed and secured, I would replace the sample head back onto the load cell. Now measurements were ready to be taken.

With the "Plot Monitor" window open, from Arduino software, I made sure that the readings were zero and that changes in values were seen only when applying force to the load cell. I would regularly check whether the load cell was functioning or not. Once everything was properly functioning, I would begin to approach the PM to the sample with the Trinamic software. I would first approach the PM until onset of the magnetic response would show and then start from there. For all experiments, steps of 13000 ($\simeq$0.5mm) from the stepper motor were displaced and readings were subsequently recorded on OriginPro. After every displacement of the PM, at least one-minute delay was waited before recording the value so that the load cell readings could adjust to the change in force. This procedure was repeated for five different samples, two from the different mixing ratios for CR131 resin, totaling to 20 individual specimens tested.

3.2.5 Finite Element Method Modeling

Finite element Method Magnetics (FEMM) 4.2 is a free software with a suite of programs for solving low frequency electromagnetic problems on two-dimensional planar and

axisymmetric domains. This program addresses linear/nonlinear magnetostatic problems, linear/nonlinear time harmonic magnetic problems, linear electrostatic problems, and steady-state heat flow problems. For our purpose, FEMM 4.2 will be utilized to validate the credibility of the MFS.

To verify the accuracy and credibility of the MFS, FEMM 4.2 was used. A known material of low carbon steel was shaved in the required shape to fit the load cell and tested using the same methodology as previously described. Measurements are recorded and plotted via OriginPro. Using FEMM 4.2, 2D planar representations of the reference PM and the sample were programmed with the correct dimensions. Both neodymium PM and low carbon steel material properties were found within the FEMM library and assigned accordingly in the schematic. Linear magnetostatic values were recorded for distances between 1-10mm every 1mm step (Appendix 7.2).

4. Results/Discussion

4.1 Scanning Electron Microscopy (SEM)

4.1.1 Soft Magnetic Powder

Figure 11 shows images of the individual Fe particles using a scanning electron microscope (SEM) after sputtering at 20 mA for 30 seconds with Au/Pd.

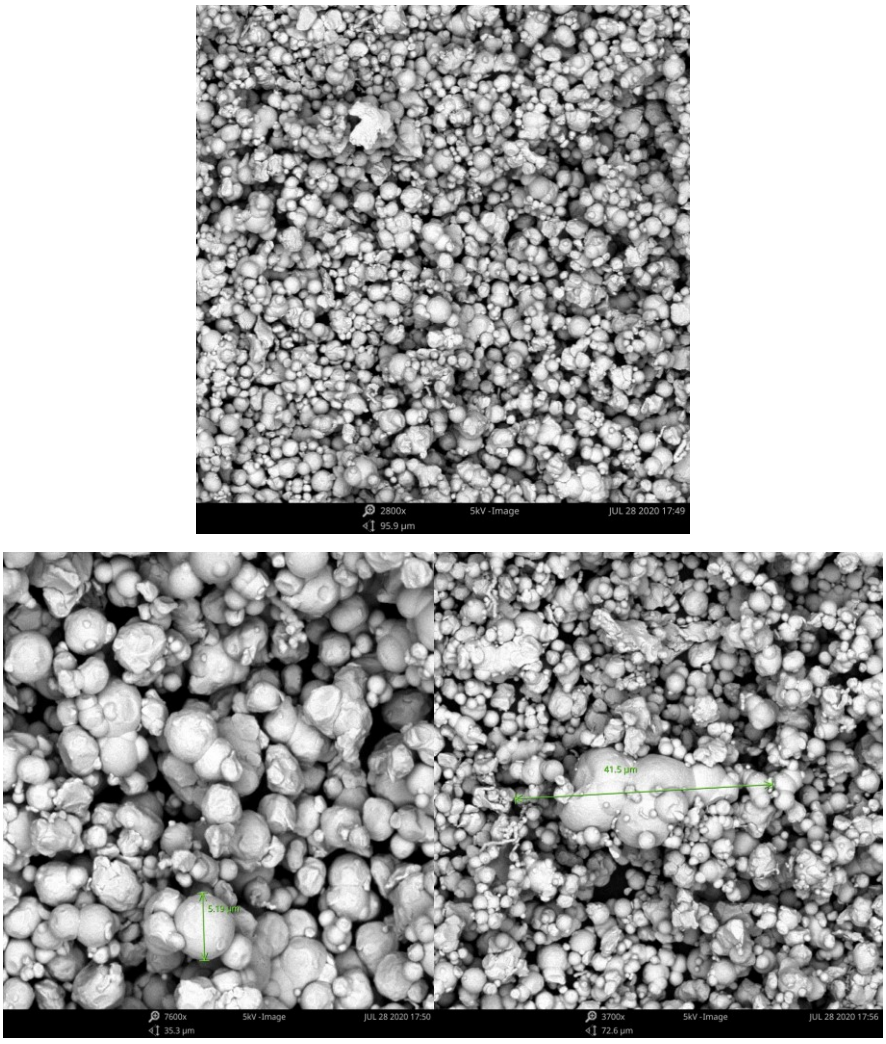

Figure 11: Fe particles SEM images, **top**.) 2800x magnification; **left**.) 7600x; **right**.) 3700x

As you can see Figure 11 (top), the Fe powder is spherical in shape and nature, while the sizes vary slightly. Figure 11 (left) shows the rough measurement of a random particle as 5.19 μm. This Fe particle displays the exact shape (minus the little extra piece attached to it) which would benefit the quality of the SMC greatly. Perfectly spherical is the ideal case because of both the direction of the magnetic field density and for its structurally sound shape. The average size seemed to be around 5 microns however, there were cases of diameters ranging up to 40 μm. This can be seen in Figure 11 (right), which represents the least ideal case.

4.1.2 CR131-based SMC

Batch 1:

The following figures below are SEM images of the samples with CR131 resin in 50/50 weight % mixing ratio. Figure 12 (left, center, right) captures the images after sputtering 20 mA for 30 seconds of Au/Pd.

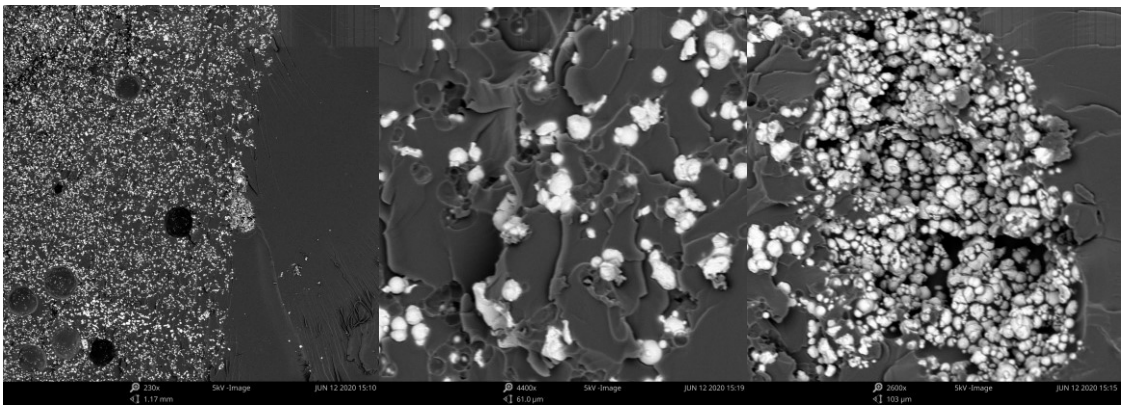

Figure 12: 50/50% CR131 SMC SEM images, **left**.) 230x magnification; **center**.) 4400x; **right**.) 2600x

Upon qualitative examination of the 50/50% (Particle/Resin) images, two distinct layers between empty resin and Fe mixture is evident as seen in Figure 12 (left). Layer on the right is clearly the empty CR131 resin while the left half is most likely a combination of Fe particles and resin which had sedimented to the bottom. This separation of resin and particle could implicate faulty results for our measurements. Another thing to note are the pores or bubbles making crater-like defects.

This most assuredly occurs during curing/heat treatment, yet there are techniques to avoid this with high performance devices such as: vacuum chambers, compressors, and mixers. These pore defects can pose future complications in terms of the mechanical properties of our SMC due to ease of crack propagations. Figure 12 (center) shows a closer view in the particle sedimented area. There seems to be poor particle distribution where certain clusters of particles are formed, while other regions of the resin are left empty. This becomes a recurring challenge throughout SMC production. However, there seems to be adequate adherence between resin and particle surface. Good coverture of resin to particles is very important for the mechanical and electrical objective of SMC. Lastly, in image 12 (right) there occurs an unwanted effect during SMC preparation in the form of particle clustering. This cluster or poor distribution of Fe particles will not only lead to core losses such as eddy current, hysteresis, and residual, but as well as a detriment to the mechanical properties of my samples.

What was qualitatively observed during preparation, where a top half of my specimens consisted of the resin while the bottom half was the Fe particles which had sedimented, is now undoubtedly apparent from these images. There is a clear separation between the settled Fe particles and the CR131 biresin. This separation is most certainly due to the lack of Fe powder amount mixed, since the resin has low viscosity there becomes sedimentation. A mixing ratio of higher than 50/50 weight % should have been used instead. The resulting samples, therefore, do not have complete homogeneity of particle distribution. In addition, there are pores or “bubble” defects apparent throughout. The pore defects could have been better avoided by using higher quality mixing/compacting processes, instead of mixing by hand, which unfortunately was left unavailable due to the closure of all labs. From one image, of one sample, it seems that there is more than adequate contact between resin and particles, with little to no gaps between. However, multiple samples would need to be imaged to make a more certain assessment. As previously stated, particle/resin binding can have either a positive or negative affect on the overall magnetic and mechanical performance of soft magnetic composites (SMC). It would be an interesting experiment, to see the overall magnetic strength of the resin dominant side versus the particle heavy loaded one, which is depicted in the results sections. Assumedly, the particle

heavy side of the sample would have a stronger reaction to the permanent magnet (PM), with respect to distance, than that of the resin dominant half.

Batch 2:

The following images (Figure 13 left, center, right) are taken with SEM of specimen with 70/30 weight percent mixing ratio after sputtering 20mA for 30 seconds of Au/Pd.

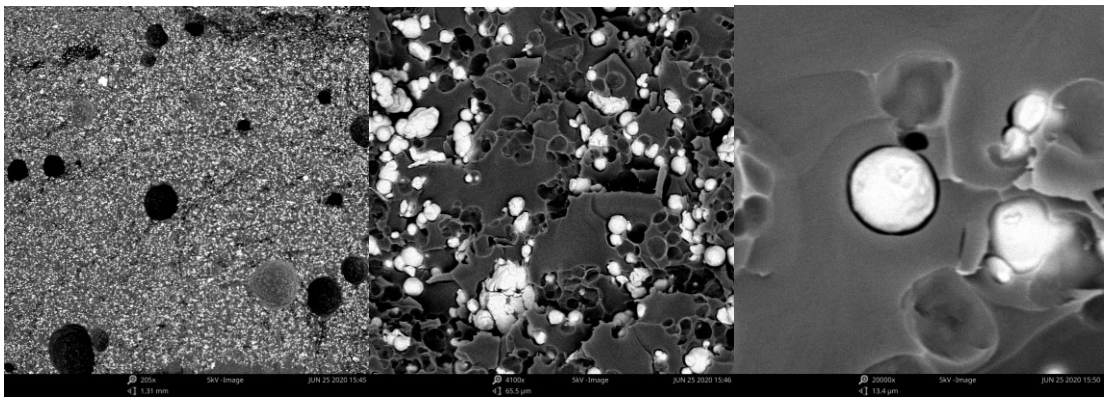

Figure 13: 70/30% CR131 SMC SEM images, **left**.) 205x magnification; **center**.) 4100x; **right**.) 20000x

Upon qualitative examination of the 70/30% (Particle/Resin) images, there is no apparent separation of resin and particle, unlike batch 1, in any of the samples. This full distribution of particles would signify a good mixing ratio for SMC production. With such full distribution, it could prove to show more enhanced properties when comparing with the previous method. Figure 13 (left) shows a very good distribution of particles throughout, however, like the previous batch there seems to be a common problem with pore defects with my samples. When taking a closer look (Fig.13 (center)), there is a better view of the particle distribution, which seems to be adequate for now. However, when it comes to the adhering between particle and resin it seems to be very poor. Figure 13 (right) is the best representation of how particle/resin contact should not look like.

Although an increased amount of Fe powder ratio is mixed for this batch, it still proves to have certain characteristics that may lead to complications during testing. For one, there are still pore defects throughout my samples. Again, there are much better methods used when attempting to reduce the number of pores but involve high caliber preparation devices. One simple method would be to leave samples in a strong enough vacuum so that the bubbles rise until the surface breaks, and then apply a heat treatment with a certain temperature that will avoid creating anymore bubbles. Another characteristic to mention, unlike the last batch, is poor contact between particle and resin. Clear gaps are noticeable which can and will lead to certain core losses and poor mechanical properties. This gap is most likely a consequence of the curing process. If temperatures are too high, and then cooled at too low of rate, then the gaps will occur due to vibrational motion of the particles. Therefore, to avoid such gaps a precise temperature while treating should be understood and implemented.

4.1.3 G/Flex-based SMC

The following are SEM images of G/Flex sample (14 left, center, right) sputtered at 20 mA for 30 seconds of Au/Pd.

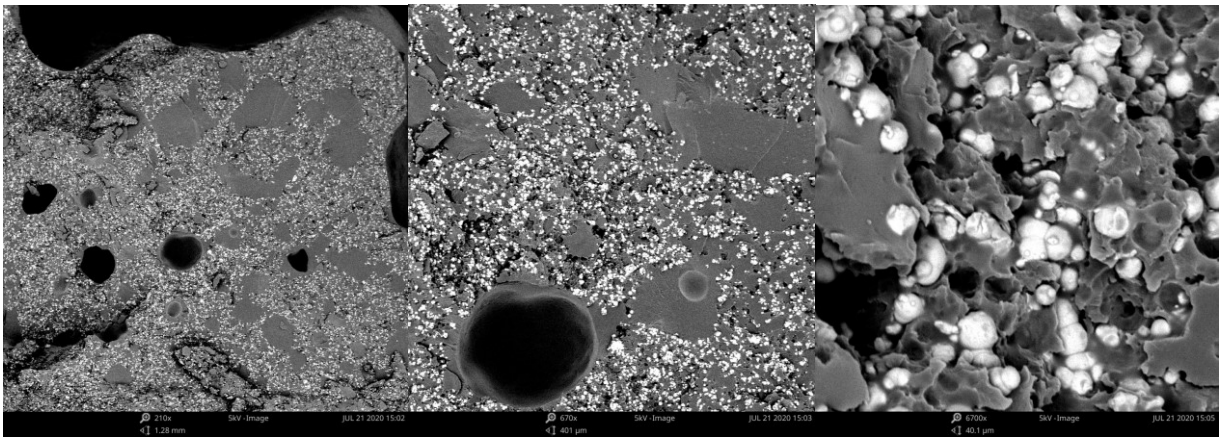

Figure 14: 70/30% G/Flex SMC SEM images, **left**.) 210x magnification; **center**.) 670x; **right**.) 6700x

Upon further analysis of the G/Flex SMC SEM images, a better descriptive understanding can be interpolated. Figure 14 (left) depicts the largest area of the samples cross section. There seems to be two distinct “pores” occurring in this sample. One is the typical pore occurring due

to bubbles during mixing/curing processes, however, these pores could also represent the area of iron that was left on the other side of the split sample. If actual pores, this would leave an area in the sample where there is no addition to the overall magnetic strength. If we take a closer look at Figure 14 (center) we can better see the two phenomena happening. The effect from pore defects caused by bubbles will pose various problems in the performance of the SMC both magnetically and mechanically. The question is, will the region lacking Fe particles pose similar or different problems and then which? A lack of Fe particles will most likely affect the magnetic performance of our samples and prove to perform poorer than that of CR131. Furthermore, the soft nature of these samples will jeopardize the structure necessary to go through mechanical examination and consequently fail. Figure 14 (right) shows the closest image of the G/Flex cross section of the sample. Showing adequate particle/resin contact with little to no gaps between, this will benefit its performance.

4.1.4 Biothan-based SMC

SEM images (15 left, center, right) taken of the cross section of the Biothan sample. Samples are sputtered at 20 mA for 30 seconds with Au/Pd.

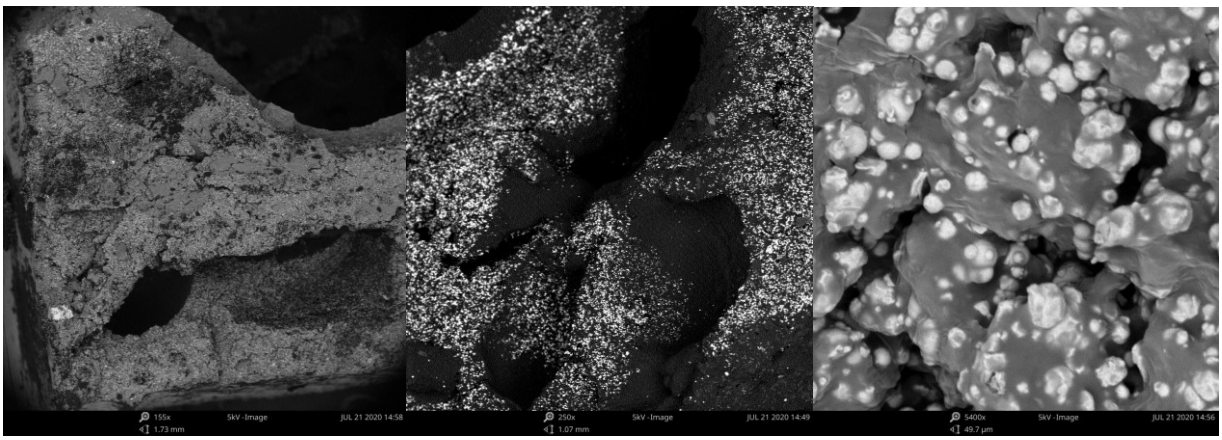

Figure 15: 70/30% Biothan SMC SEM images, **left**.) 155x magnification; **center**.) 250x; **right**.) 5400x

Figure 15 (left, center) is a wide view of the cross-sectional area of the Biothan SMC sample. As previously mentioned, the texture of these samples was very soft with higher elasticity than that of the G/Flex. Due to this softness, there is a compromise in the structure of the sample. This is

evident from these SEM images. Furthermore, there seems to be less “typical” pores, which have been seen in other SMC, but instead large fissures of material are missing. This lack of structural integrity will most likely have a negative effect on the overall magnetism of these samples. Less particles, less magnetism. However, not all is lost. Figure 15 (right) is the closest image of this sample and portrays clearly the resin/particle contact. This is the most ideal surface contact coverage observed in the studied samples. As you can see the individual particles are completely covered by the resin. This means that there is little to no gaps at all, which indicates a better chance of avoiding large amounts of core losses such as: hysteresis, eddy current, and residual.

4.2 Finite Element/Analytical Analysis

Below is an example of the magnetic density plots created using FEMM software.

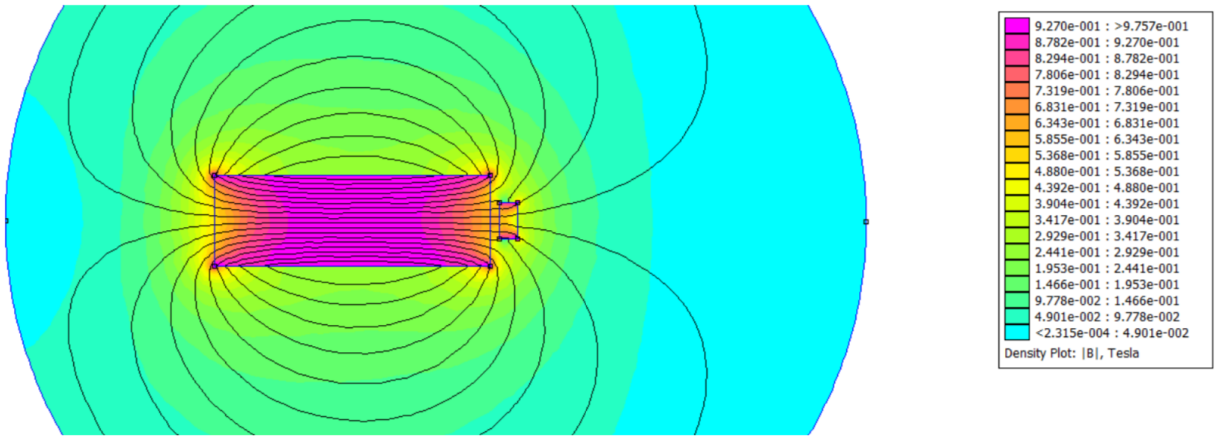

Figure 16: Magnetostatic force density plot for low carbon steel (right block) 1mm away from neodymium PM (left block), Force= 8.61581 N (Appendix 6.2.a)

Table 3: Force with respect to Distance Between Steel & PM

Distance (mm)	Force (N)	Appendix 7.2
1	8.61581	a
2	6.07113	b
3	4.17205	c
4	2.86516	d
5	1.98390	e
6	1.38674	f
7	0.978147	g
8	0.709581	h
9	0.519109	i
10	0.385565	j

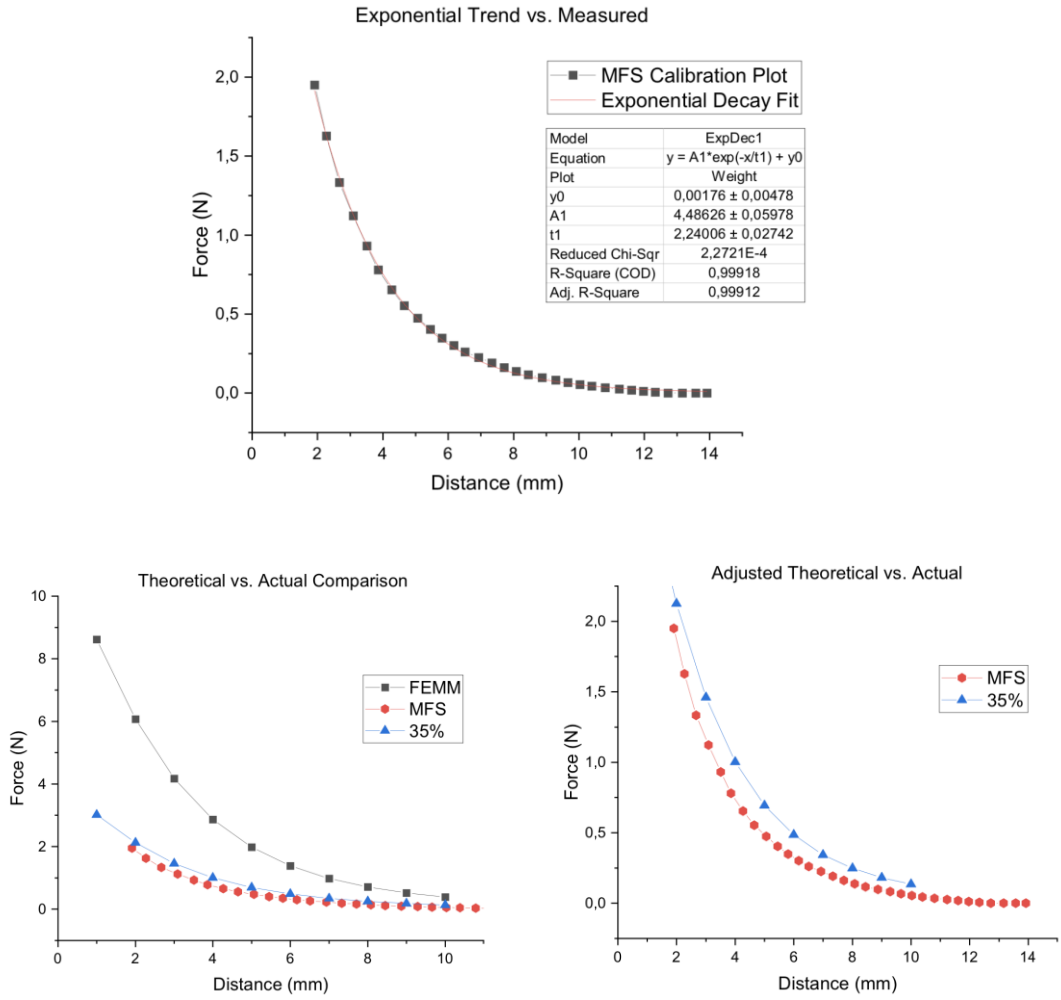

Figure 17: **top**.) Exponential fit plot; **left**.) Force vs. Distance plot for theoretical (black), actual (red), and recalculated theoretical (blue); **right**.) Force vs. Distance plot for theoretical (red), recalculated theoretical (blue)

As clearly seen in Table 3, which shows the theoretical values gained from the FEMM software, as the distance between the permanent magnet (PM) and steel sample increases, the magnetic force decreases. The strongest value was recorded at 1 mm (8.62 N), while the furthest value measured at 10 mm was 0.39N. With these values we can now compare with those taken with the MFS device.

Figure 17 (left) shows exactly that comparison. What it portrays is the magnetic strengths of the results from both theoretical, actual, and adjusted theoretical value as a function of distance. The actual values were converted from grams to Newtons beforehand. The curves seemed to follow an exponent trend, therefore, a fit curve was applied and proved (Figure 17 (top)) an R-square value of 0.99. This validates that these curves follow an exponential trend and can from now on be considered as so. This was to be expected since Equation 4 has a degree two polynomial. As seen in Figure 17 (left), the MFS overall magnetic strength values (in red) are weaker than the theoretical values (in black). However, this disparity between results can be explained and accounted for. A major discrepancy seen between MFS and theoretical plots are due to the lack of the FEMM software capabilities. That is, the model could only be rendered in 2D and not 3D. Therefore, there is no ability to replicate the exact sample shape as is shown in Figure 11. Therefore, there are area dissimilarities, bringing us back to Equation 4 where area as well influences the resulting magnetic strength. The smaller the area, the smaller the magnetic field strength will be which is now corroborated even further with Figure 17 (left).

Upon this realization, after calculating both the theoretical and actual areas, I then calculated the percent difference so that it could be accounted for and applied this value to my results. Since the area of one sample ($83mm^2$) was 35% that of the theoretical one (240 mm^2), the theoretical values of the force were adjusted by a factor of 0.35. This adjustment was then plotted and seen represented as the blue plot in Figure 17 (left). As you can see, the blue plot matches much more closely that of the actual value (red). Figure 17 (right) displays a closer look at the comparison between these two values. The two curves are in good agreement with each other with a close fit. This is exactly what was needed to validate the legitimacy and accuracy of the magnetic force sensor (MFS). With this proof, the MFS can now be used to test my SMC samples.

4.3 Magnetic Force Measurement

4.3.1 CR131-based SMC

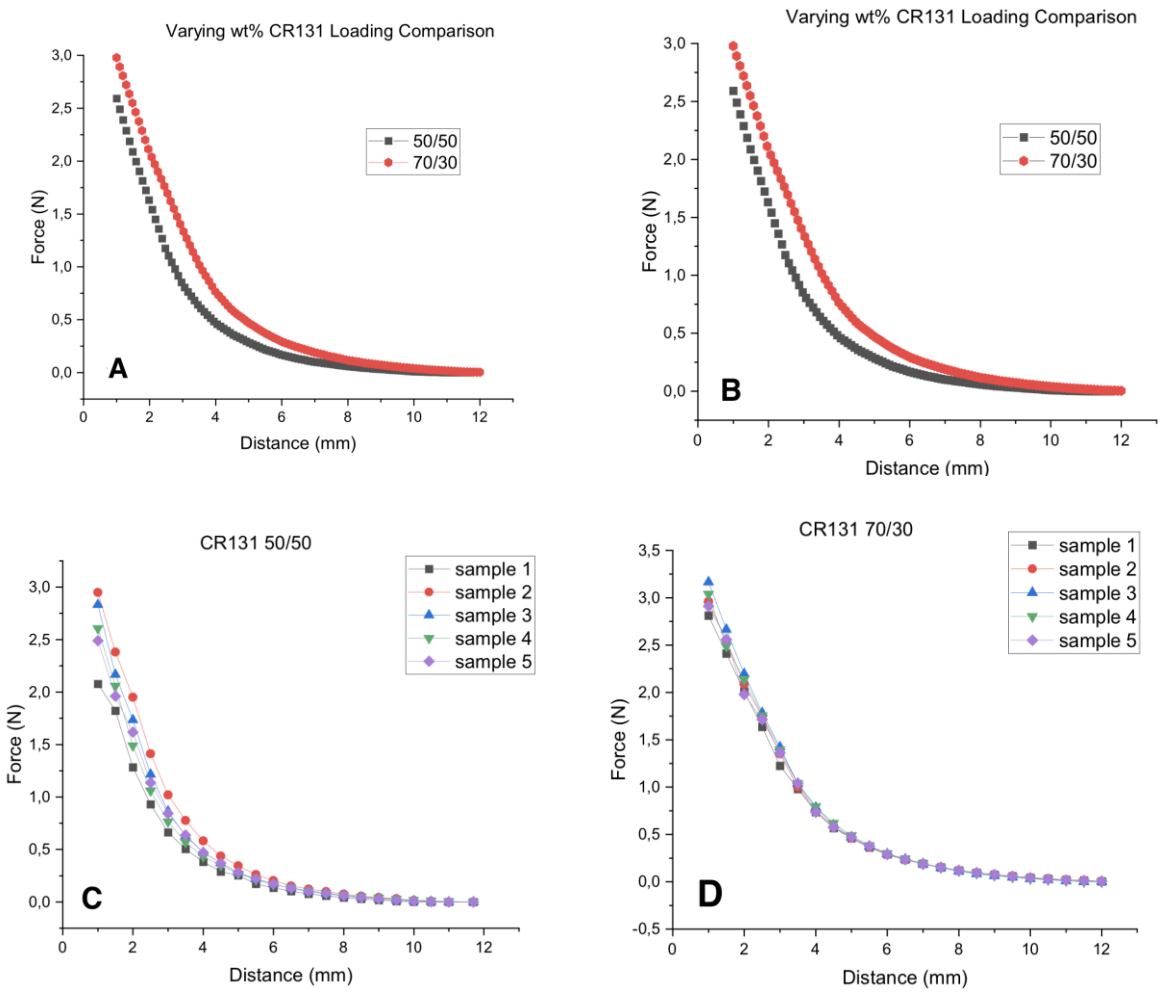

Figure 18: **A**.) Resin vs. Particle heavy SMC sample side; **B**.) Average force-distance plots between CR131 50/50 loading (red) and 70/30 (black); **C**.) Magnetic Force Plot for 50/50 CR131 SMC specimens; **D**.) For 70/30

As previously mentioned for batch 1, it was of intrigue to further investigate the magnetic strength from one side (resin) of the SMC samples and compare it with the other side (particles). It was hypothesized that the particle heavy side would display stronger forces. Hence, using one sample only, Figure 18(A) depicts the answer to this hypothesis. As you can see, the magnetic

attraction between the resin dominant sample side and the permanent magnet (PM) has a weaker force, as a function of distance, than that of the particle loaded sample. This corroborates with my previous assumption. With this knowledge in mind, I decided from then on to use the particle heavy side of the samples when taking measurements with the magnetic force sensor (MFS). Figure 18(C) represents the exponential trend for five samples from the 50/50 weight percent ratio of CR131 (batch 1).

A common tendency throughout my various measurements, which should be addressed now since it is present in these plots, are that the values between 4-6mm tend to align with great precision, while below these distances they diverge. This, in fact, must do more with the MFS device than the samples themselves. Detailed further in Appendix 6.1, the device uses a 500g strain gauge load cell to convert the voltage difference, from bending, into readings of force. However, the employed load cell suffers from creep, noise, and poor response. Yet, these issues seem to have predominantly occurred when reaching this critical point of 4mm and worsen as it decreased. Hence, in an attempt to maintain stability, certain reading techniques were used to minimize as much loss of precision as possible between these ranges, which included: restarting the program before every new sample measurement and rounding value readings once at 4mm and approaching. This also accounts for the reason why I measured five samples from each varying resin, so that it would allow an average between plots to be taken and compared.

So, as you can see in Figure 18(C), five samples were measured and plotted. The values align quite well between 4-6mm yet diverge below. Initial readings were measured as far as 12mm and as high as 3N. While for 18(D) the readings seem to start a bit further than 12mm and reach values above 3.5N. Yet, it is in Figure 18(B) where we see a comparison between batch 1 (50/50) and batch 2 (70/30). As stated, it seemed most likely that batch 2 will have a stronger response to the PM with respect to distance and Figure 18(B) now verifies it. Thus, demonstrating the importance that mixing ratio has when it comes to the magnetic quality of SMC. Since the following measurements for different resin also used 70/30 weight percent mixing ratio, only batch 2 will be used for the final comparison of all resins.

4.3.2 G/Flex Plot

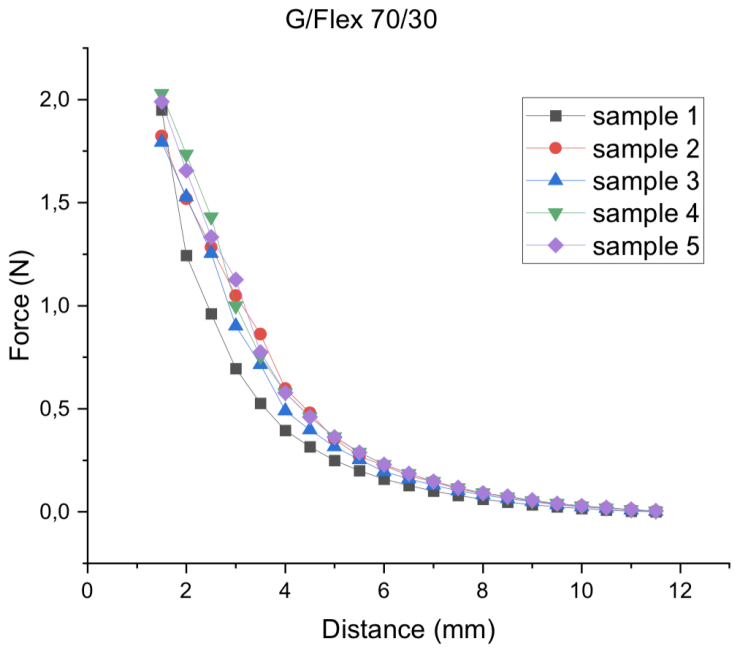

Figure 19: Magnetic Force Plot for 70/30 G/Flex SMC samples

Figure 19 displays the force-distance plots for five specimens of G/Flex-based SMC with 70% Fe. Initial readings begin as far as 12mm and reach as high as 2N. Immediately, when comparing to CR131 (Figure 18), there is a noticeable difference in the amount of strength in weight one has over the other. Where CR131 reaches values up to 3.5N, compared to 2N attained by G/Flex. In fact, even CR131 with only 50 wt% of particles (Figure 18(C)) reached higher values than G/Flex with 70 wt% of particles. This begs the question as to why and how is this possible? The only material, which has any magnetic properties, comes from the Fe particles. Therefore, when mixing equal amounts, we should obtain equal values. This then leads me to wonder if the resin has anything to do with the effect on the permeability of the iron cores. Does it distort its flux density or perhaps react differently to an external magnetic field while a binder is in between? However, this is only a hypothesis and would need to be assessed once measurements for all varying resin-based SMC are compared.

4.3.3 Biothan Plot

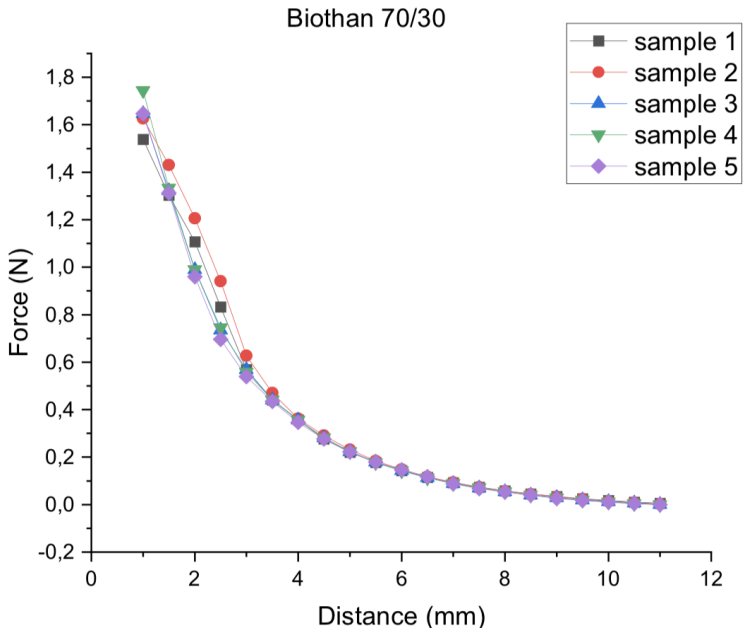

Figure 20: Magnetic Force Plot for 70/30 Biothan SMC samples

In Figure 20 we see five unique exponential trends between 70/30 weight percent Biothan SMC samples. Initial readings begin below 12mm and strength of around 1.8N. There seems to be an even weaker reaction, in terms of magnetic strength, to the PM than compared with resins CR131 and G/Flex. This weakness in force could pertain to the SEM images (Figure 15), which demonstrated a lack of particles, due to a lack of structural integrity. Leading me to suspect that this is the most likely reason for a weaker strength.

4.3.4 Overall Comparison Plot

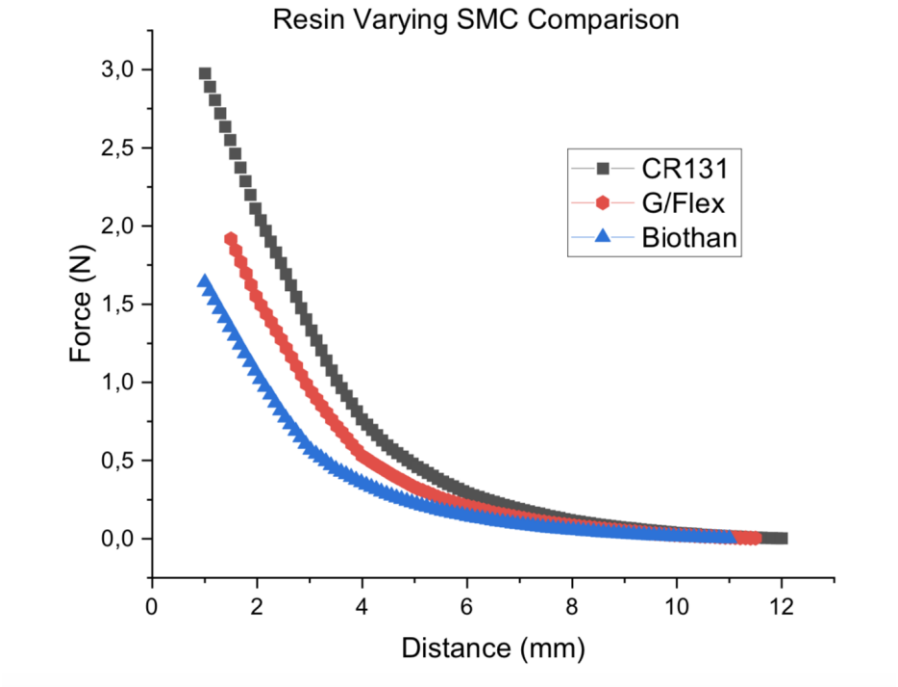

Figure 21: Average Magnetic Force Plot for CR131, G/Flex, and Biothan SMC samples

Figure 21 shows the average curves taken from each set of unique SMC resin, measured and compared. Resin CR131 shows to have the strongest reaction to the PM with an initial response occurring from over 12mm away and reaching a strength of over 3.5N, while the weakest response comes from Biothan. However, unfortunately, this outcome is not surprising. The cause for such disparity comes assuredly from the quality of my SMC samples for Biothan and G/Flex, which came out as more defective. Not only were there too many pores but the softness of the samples made them extremely vulnerable to breaking. In fact, there were times when the shear magnetic strength of the PM would cause the samples to split in half. Therefore, it cannot be deduced whether the different resins have an effect on the permeability of the samples or even distort magnetic flux somehow from these graphs alone.

If the samples were not missing large quantities of Fe particles within its structure, the results would be better suited for comparison. This failure, as stated, is due to how the samples were prepared. It rather proves how difficult and meticulous sample preparations can be for SMC production, especially without the proper equipment. There are too many uncontrollable variables during the process such as: particle distribution/uniformity, correct temperature for curing, and pore defects (bubbles) avoidance, to list a few. However, this only further proves the capabilities of the magnetic force sensor (MFS). What was qualitatively apparent with the defects of the samples, was quantitatively proven through the functionality of this device. Therefore, giving reason to perhaps optimize the system even further.

There were many areas of the device which most likely impacted the results negatively. For one, making sure that the permanent magnet (PM) is exactly level with our samples. The uneven distribution of the magnetic flux densities could skew the force readings somehow. Next, the sample holder should include a system which fixes the sample in place more tightly. The samples themselves fit perfectly into the slot of the 3D printed part however, not tight enough from keeping them from flying out towards the PM. Lastly, and most importantly, change the load cell in terms of max weight capacity and quality. The 500g capacity of this load cell was just right. However, although none of my measurements reached such forces, 300g was met quite easily and thus should be considered for future tests. Finally, quality of the load cell has a significant role in the accuracy of the values. Noise, creep, and faulty calibration are all issues which occur more frequently with cheap load cells. An addition to the quality of the load cell, would be the transmitter as well. Making sure readings are stable and accurate will occur with a transmitter intended for such load cell purposes, rather than transmitted through an Arduino (Appendix 7).

5. Conclusions

In the present thesis, soft magnetic composites (SMC) were prepared and studied using a magnetic force sensor (MFS) device, constructed by me, with a limited amount of resources. Its capabilities as a functionable device was proven using a finite element method (FEM) software. Three different resins were used to make varying SMC samples: CR131, G/Flex, and Biothan. The magnetic attraction between samples and a permanent magnet (PM), was measured with the MFS as a function of distance. SMC samples with CR131 resin proved to show the strongest response to the PM while Biothan the weakest. This was not unexpected due to the quality of my samples, which were further proven using scanning electron imaging (SEM). Throughout the images, pore like defects were prevalent. These pores indicate volumes of space lacking Fe particles which will assuredly reduce the magnetic effect of the samples. However, when it came to particle/resin contact, it seemed that it was more than adequate with Biothan showing ideal coverage. Although this does not significantly affect the magnetic properties of our samples, it could indicate the difference between good and poor mechanical properties, which is an important factor when working with SMC. Further optimization of both sample preparation and the MFS device itself should be implemented for more accurate results. Better quality devices and techniques should be used when preparing samples, so to avoid pores and defects, while a better load cell and minor adjustments to the MFS should be made for better readings. Once these adjustments are made, a better understanding of the effect resin has onto magnetic cores can be studied. However, the production processes of SMC are already controlled and properly executed industrially for quality parts, yet there needs to be further optimization of particle distribution before the use of this material becomes widely acceptable.

5.1 Future Work

The performed research work has demonstrated the potential of creating a cost-effective device that can accurately measure the magnetic performance of SMC samples with limited resources and time. However, a big part of SMCs appeal is also in its mechanical properties in unison with its magnetic ones. Therefore, for future projects the construction of a cost-effective

tensile/fatigue device using approximately the same design as the MFS could be made. This device would include a stepper motor as well but with an s-type load cell instead. Furthermore, optimization of the MFS could prove beneficial such as: replacing the existing load cell with one of better quality, using a transmitter for the exact purpose of reading measurements rather than use an Arduino, and perhaps enlarge the device so that it can test bigger samples.

Once magnetic and mechanical processes are optimized, it could be further possible to test its capabilities with an actual application. For example, SMC made using optimized procedures could be shaped into any parts which could be implemented into a flywheel. For the purposes of a flywheel, the SMC would be implemented in the active magnetic bearing portion of the machine. This area of the machine is involved with the important task of magnetically stabilizing the levitated rotor as it spins extremely fast. The destructive nature of the device could prove disastrous if the soft magnetic composites are not effectively made.

6. References

[1] "6.8: Ferro-, Ferri- and Antiferromagnetism." Edited by Libretexts, *Chemistry LibreTexts*, Libretexts, 11 Feb. 2020, chem.libretexts.org/Bookshelves/Inorganic_Chemistry/Book%3A_Introduction_to_Inorganic_Chemistry/06%3A_Metals_and_Alloys-_Structure%2C_Bonding%2C_Electronic_and_Magnetic_Properties/6.08%3A_Ferro-%2C_Ferri-_and_Antiferromagnetism.

[2] "8.3: Orbital Magnetic Dipole Moment of the Electron." *Physics LibreTexts*, Libretexts, 13 July 2020, phys.libretexts.org/Bookshelves/University_Physics/Book%3A_University_Physics_(OpenStax)/Map%3A_University_Physics_III_-_Optics_and_Modern_Physics_(OpenStax)/08%3A_Atomic_Structure/8.03%3A_Orbital_Magnetic_Dipole_Moment_of_the_Electron.

[3] "A000066 - Development Board, Arduino Uno, ATmega328P MCU, 14 3.3V I/O, 6 Analogue Inputs, 6 PWM Outputs." *Farnell*, fi.farnell.com/arduino/a000066/arduino-uno-evaluation-board/dp/2075382.

[4] "Antiferromagnetism." Edited by The Editors of Encyclopaedia Britannica, *Encyclopædia Britannica*, Encyclopædia Britannica, Inc., 22 Sept. 2011, www.britannica.com/science/antiferromagnetism.

[5] ATRIVIO GmbH media network, Kempten Germany. "Optimal Use of SMC in Electric Machines." *PMG*, 2 July 2020, www.pmgsinter.com/1818.htm.

[6] Beltramin, Laura. "State-of-the-Art of the Flywheel/Li-Ion Battery Hybrid Storage System for Stationary Applications." *University of Padova/ State of the Art Flywheel Technology*, *Università degli Studi di Padova*, 2018, tesi.cab.unipd.it/61871/1/Beltramin_Laura_1148147.pdf.

[7] "Biresin® CR131 Biresin-cr131." *Sika Advanced Resins*, advanced-resins.sika.com/content/sikaaxson/usa/en/products_solutions/product-groups/composite-resin-systems/composite-resin-systems-for-vacuum-infusion/biresin-cr131.html.

[8] Chaudhry, MS, and Matias Sotomayor November 18. "Explanation of Hysteresis Loss & Eddy Current Losses in Transformers." *Electrical Engineering 123*, 9 Sept. 2016, electricalengineering123.com/explanation-of-hysteresis-loss-eddy-current-losses-in-transformers/.

[9] *Classes of Magnetic Materials*, www.irm.umn.edu/hg2m/hg2m_b/hg2m_b.html.

[10] "Effects of Heat Treatment and Lubricant on Magnetic Properties of Iron-Based Soft Magnetic Composites with Al2O3 Insulating Layer by One-Pot Synthesis Method." *ResearchGate*.

[11] "Electric Charge." Edited by Erik Gregersen, *Encyclopædia Britannica*, Encyclopædia Britannica, Inc., 27 May 2020, www.britannica.com/science/electric-charge.

[12] "Ferromagnetism." *Questions and Answers in MRI*, www.mri-q.com/what-is-ferromagnetism.html.

[13] "Form 2: Affordable Desktop SLA 3D Printer." *Formlabs*, formlabs.com/eu/3d-printers/form-2/.

[14] *Getting Started with Load Cells*, learn.sparkfun.com/tutorials/getting-started-with-load-cells/all.

[15] "Hochleistungs-Polymere Für Bewegung." *Igus*, www.igus.de/.

[16] "Hysteresis." *Hysteresis in Magnetic Materials*, hyperphysics.phy-astr.gsu.edu/hbase/Solids/hyst.html.

[17] info@micro-epsilon.de, Micro-Epsilon Messtechnik -. *Compact Laser Triangulation Displacement Sensor*, www.micro-epsilon.com/displacement-position-sensors/laser-sensor/optoNCDT_1320/?sLang=en.

[18] Instructables, DegrawSt. "Arduino Scale With 5kg Load Cell and HX711 Amplifier." *Instructables*, Instructables, 13 Apr. 2019, www.instructables.com/id/Arduino-Scale-With-5kg-Load-Cell-and-HX711-Amplifi/.

[19] "Iron 255637 Specifications." Edited by Merck, *Sigma Aldrich*, www.sigmaaldrich.com/catalog/product/aldrich/255637?lang=fi®ion=FI.

[20] Johnson, Todd. "Learn the Difference Between Thermoplastic and Thermoset Resins." *ThoughtCo*, 2020, www.thoughtco.com/thermoplastic-vs-thermoset-resins-820405.

[21] Larsson, Oskar. "Fe-Based Amorphous Powder for Soft-Magnetic Composites." *Department of Material Science and Engineering Royal Institute of Technology*, 2013, www.diva-portal.org/smash/get/diva2:630121/FULLTEXT01.pdf.

[22] "Lorentz Force - Definition, Formula & Applications." Edited by Admin, *BYJUS*, BYJU'S, 8 July 2020, byjus.com/physics/lorentz-force/.

[23] "Lorentz Force." Edited by Erik Gregersen, *Encyclopædia Britannica*, Encyclopædia Britannica, Inc., 27 May 2020, www.britannica.com/science/Lorentz-force.

[24] Madhu. "Difference Between Magnetic Permeability and Susceptibility." *Compare the Difference Between Similar Terms*, Differencebetween.com, 9 Apr. 2018, www.differencebetween.com/difference-between-magnetic-permeability-and-vs-susceptibility/.

[25] "Magnetic Materials: Soft Magnets." Edited by Birmingham University, *University of Birmingham*, www.birmingham.ac.uk/Documents/college-eps/metallurgy/research/Magnetic-Materials-Background/Magnetic-Materials-Background-10-Soft-Magnets.pdf.

[26] "Magnetic Permeability." *Encyclopædia Britannica*, Encyclopædia Britannica, Inc., 6 May 2020, www.britannica.com/science/magnetic-permeability.

[27] Mulia, Edison. "Global Consumer Technology Market: Key Trends and Investment Landscape." *EqualOcean*, EqualOcean, 25 Nov. 2019, equalocean.com/high-tech/20191123-analysis-on-global-consumer-technology-market-and-investment-trend.

[28] Oikonomou, Christos. *On Surface Characteristics and Microstructural Development of Soft Magnetic Composite Powder and Components*, *Chalmers University of Technology, Gothenburg Sweden*, Chalmers Reproservice, 2015, pp. 1–51, http://publications.lib.chalmers.se/records/fulltext/224726/224726.pdf

[29] Perigo, Elio Alberto, et al. "Past, Present, and Future of Soft Magnetic Composites." *Research Gate*, July 2018, www.researchgate.net/publication/326658217_Past_present_and_future_of_soft_magnetic_composites.

[30] "The Properties and Effects of Manganese as an Alloying Element." *AZoM.com*, 19 Apr. 2019, www.azom.com/article.aspx?ArticleID=13027.

[31] "QSH5718." *Trinamic*, www.trinamic.com/products/drives/stepper-motors-details/qsh5718/.

[32] Ritchie, Hannah, and Max Roser. "Energy." *Our World in Data*, 28 Mar. 2014, ourworldindata.org/energy.

[33] Shi, Donglu, et al. *Nanomaterials and Devices*. William Andrew Applied Science Publishers, 2015.

[34] Shokrollahi, H., and K. Janghorban. "Soft Magnetic Composite Materials (SMCs)." *Journal of Materials Processing Technology*, Elsevier, 24 Feb. 2007, www.sciencedirect.com/science/article/abs/pii/S0924013607001756.

[35] "Soft Magnetic Applications Guide." Edited by Arnold Magnetics, *Arnold Magnetics Technologies*, 2015, www.arnoldmagnetics.com/wp-content/uploads/2017/10/FINAL_Tech-Library_Guides_Soft-Magnetics-Application-Guide.pdf.

[36] "SparkFun Load Cell Amplifier - HX711." *SEN-13879 - SparkFun Electronics*, www.sparkfun.com/products/13879.

[37] "G/Flex 650 Toughened Epoxy • Permanent, Waterproof." *WEST SYSTEM*, 28 Oct. 2019, www.westsystem.com/specialty-epoxies/gflex-650-toughened-epoxy/.

[38] "Biothan for Electrical Industry." July 20, 2020, http://www.silitech.ch/d/detail_produit.asp?id_produit=283.

[39] "Thermoset vs. Thermoplastics." Edited by Modor Plastics, *Modor Plastics*, 22 Mar. 2017, www.modorplastics.com/plastics-learning-center/thermoset-vs-thermoplastics/.

[40] "Understanding Coercivity - Ideal Magnet Solutions Knowledge Base." *Ideal Magnet Solutions*, 15 Oct. 2018, idealmagnetsolutions.com/knowledge-base/understanding-coercivity/.

[41] "University Of Texas At Austin Flywheel Spins To A Milestone Speed Record." *ScienceDaily*, ScienceDaily, 14 Nov. 2003, www.sciencedaily.com/releases/2003/11/031114071848.htm.

[42] Weidenfeller, B., et al. "Preparation and Characterisation of Soft Magnetic Composites Based on Fe Fibres." *Journal of Materials Science*, Springer US, 1 Jan. 1970, link.springer.com/article/10.1007/s10853-019-04088-1.

7. Appendices

7.1 Magnetic Force Sensor Mechanics

7.1.1 Introduction

The purpose of this device is to determine the magnetic strength of our specimens as an initial test before using higher quality magnetometer devices. The idea is to have our sample specimen linearly approach a permanent magnet (PM), and record measurements in grams as a function of distance. A PM is a perfect reference due to the fact that its magnetic domains are unaffected by the weak forces exhibited from the SMC sample. For example, rare earth magnets are not as likely to experience instability in magnetic domains because of their extremely high coercivity, therefore the choice for the setup. As our sample approaches the PM, the force acting between the two will be measured using a load cell.

7.1.2 Load Cell/Microcontroller

To measure the forces acting between sample and PM, a strain gauge load cell was used. Strain gauge load cells have a mechanical element where when torque is applied in a certain direction four strain gauges on the cell will measure the bending distortion, two measuring compression and two tension. When these four strain gauges are set up in a Wheatstone bridge formation, it is easy to accurately measure the small changes in resistance as shown in Figure 22:

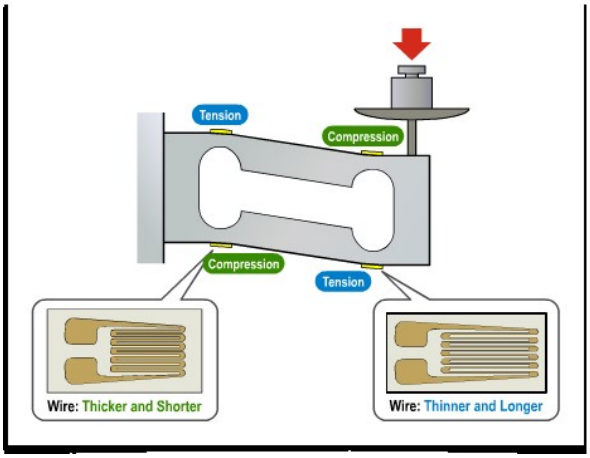

Figure 22: In depth diagram of strain gauges on bar load cells when force is applied (7)

The reasoning/counter argument to using a load cell, rather than a hall effect sensor or magnetic field sensor (MEMS), is due to the fact that with respect to measuring magnetic forces there is a limited amount of literature where the measurements are recorded in Newtons or grams rather than Tesla for flux density. Furthermore, our SMC specimens will as well undergo mechanical stress, tensile and fatigue testing, which will also be measured in Newtons. Therefore, compared measurements in Newtons could prove a potential relation between mechanical and magnetic strengths or lead to other experimental inquiries.

When connected to a digital microcontroller, the load cell is measured from resistance in the form of an analog voltage output signal which can then be converted into kilogram or Newtons. For this device a 500g bar load cell was purchased from Digikey (37).

Figure 23: Mini straight bar load cell (500 grams)

However, the change in resistance of the load cell is so small that to accurately read the signal output, a load cell amplifier is required. For this purpose, an HX711 load cell amplifier was also purchased from Digikey (37).

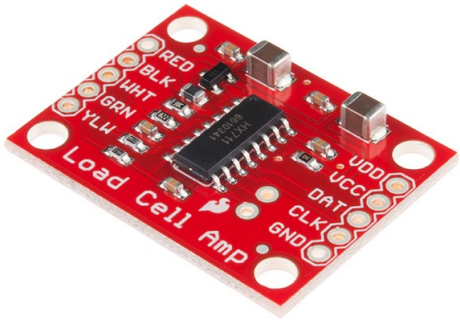

Figure 24: HX711- Load Cell Amplifier (14)

The digital board connected to both HX711 and load cell, is an Arduino Uno. Arduino is an open-source microcontroller board equipped with sets of digital and analog input/output pins that may be interfaced to various expansion boards and other circuits.

Figure 25: Arduino Uno microcontroller (3)

To power up an Arduino Uno it simply needs a 5V power supply, which is easily provided with an A to B cable or “printer cable” connected to any computer. Now to explain the details of connection and code.

7.1.3 Fritzing

There are four wires directly connected to the load cell, each with a unique color. Depending on the color is where the wires should be connected, via soldering, to the HX711 load cell amplifier.

- Red (Excitation+ or VCC)
- Black (Excitation- or GND)
- Green (Amplifier+, Signal+ or Output+)
- White (Amplifier-, Signal- or Output-)

A major complication arose due to how thin the load cell cables are. The thinness causes a poor connection, which will result in imprecise readings. Additionally, due to the thinness, the wires are more susceptible to breaking off of the load cell if not handled with care, which I personally experienced. To solve this issue, simply soldering thicker wires to the thinner wires will allow both stronger connection and ease of handling.

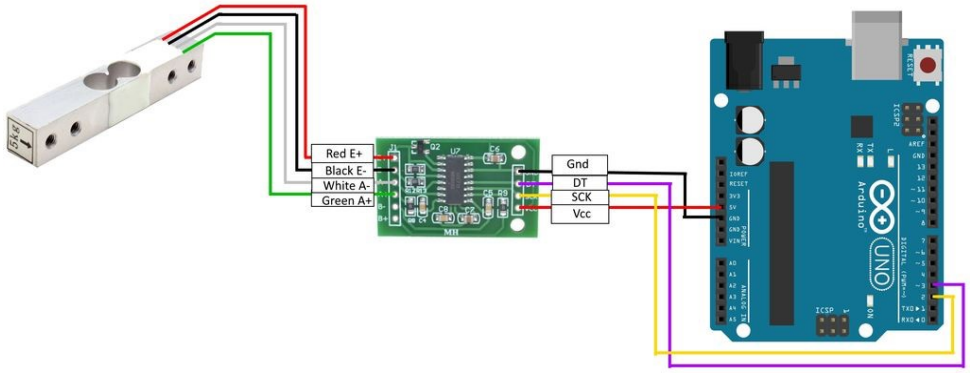

Figure 26: Scheme between Arduino, HX711 and load cell (19)

Once the load cell is properly connected to the HX711 load cell amplifier, it is now time to connect with the Arduino Uno. To make connections simpler and more reliable, solder header pins to the ports on the other side of the HX711. This allows the ease of simply using “male to female” jumper wires to the microcontroller. Figure 26 shows the final connection diagram for all components. Now to implement the code.

7.1.4 Arduino Code

```
#include <HX711.h>

#define DOUT  3
#define CLK  2

HX711 scale;

float calibration_factor = 3211; //-7050 worked for my 440lb max scale setup
float units;
float ounces;

void setup() {
  Serial.begin(9600);
  Serial.println("HX711 calibration sketch");
  Serial.println("Remove all weight from scale");
  Serial.println("After readings begin, place known weight on scale");
  Serial.println("Press + or a to increase calibration factor");
  Serial.println("Press - or z to decrease calibration factor");

  scale.begin(DOUT, CLK);
  scale.set_scale();
  scale.tare(); //Reset the scale to 0

  long zero_factor = scale.read_average(); //Get a baseline reading
  Serial.print("Zero factor: "); //This can be used to remove the need to tare the scale. Useful in permanent scale projects.
  Serial.println(zero_factor);
}

void loop() {

  scale.set_scale(calibration_factor); //Adjust to this calibration factor

  Serial.print("Reading: ");
  units = scale.get_units(), 10;
  if (units < 0)
  {
    units = 0.00;
  }
  ounces = units * 0.035274;
  Serial.print(units);
  Serial.print(" grams");
  Serial.print(" calibration_factor: ");
  Serial.print(calibration_factor);
  Serial.println();

  if(Serial.available())
  {
    char temp = Serial.read();
    if(temp == '+' || temp == 'a')
      calibration_factor += 10;
    else if(temp == '-' || temp == 'z')
      calibration_factor -= 10;
  }
}
```

Figure 27: This was the exact code I used for every experiment

7.1.5 Calibration Instructions

There is a myriad of open source projects, related to load cells, which can easily be found online for guidance. In fact, on the website where the HX711 load cell amplifier is purchased, it will most likely include sample codes with instructions to help one setup and calibrate the load cell. The sample code I used was from the Sparkfun website (14). First, download the Arduino software, which is Mac, Windows, and Linux compatible. As soon as it is downloaded, simply copy/paste the code into the programming window. For the code to properly function, it is required to download the "<HX711.h>" from Arduino's library. Simply click "Sketch> Include Library> Manage libraries", search for "HX711 Arduino Library" and then proceed to Install.

From this point on everything should work accordingly, assuming hardware connection is correct. Make sure that your "DOUT" and "CLK" numbers correlate to the exact pins connected on the Arduino microcontroller. Click "Verify" to check whether the code functions and then "Run" to begin the calibration process. There were moments when the code would not work because the USB serial port was not the correct one plugged in. To fix this either change the settings or simply unplug and plug into the correct port.

Once code is running, click "Tools> Serial Monitor" to open the window where your numerical values are shown. From the code I've chosen to use, the values are already represented in grams. The numerical values will be updating at a rate of milliseconds. An option to slow this down, simply include a "DELAY" function within the code where for example "delay (1000)" will update the values once per second. Now it's time to calibrate the load cell, where the calibration factor will be unique for every load cell.

The load cell must be properly secured somehow, so that it is as stable as possible. There are threaded screw holes on one of the sides of the load cell for ease of fixing to a platform. As long as the load cell is secure on one side, and there is space beneath the load cell on the other side, it will be possible to accurately weigh the load. Using calibration weights, or an item where the exact weight is known, place the item on the side of the load cell which is not secured. At this

point, whatever values are reading on the Serial Monitor should change. If your values are anything other than “0”, then it’s a connectivity issue and not software. Using the calibration function implemented within the code, enter “a”/”+” to increase or “ z”/”-” to decrease the values by 10. Increase or decrease until the values reading on the monitor equals the weight of your item. Once the values are equal, the load cell should be calibrated and ready to use. For my load cell the calibration factor was “3211”. However, it is imperative that the calibration factor of the system be checked regularly.

7.1.6 Magnetic Force Sensor Assembly (MFS)

A wide range of resources were used for the assembly of my setup. The resources in play were either purchased online or already accessible to me. Included below is a list of the exact parts/devices used for constructing this prototype and below is an actual image of my device:

1. Drylin® lead screw table (15)
2. Nema 23 stepper motor
3. optoNCDT laser displacement sensor (triangulation) (18)
4. Shaft coupler (for stepper motor)
5. 3D printed parts
6. Load Cell

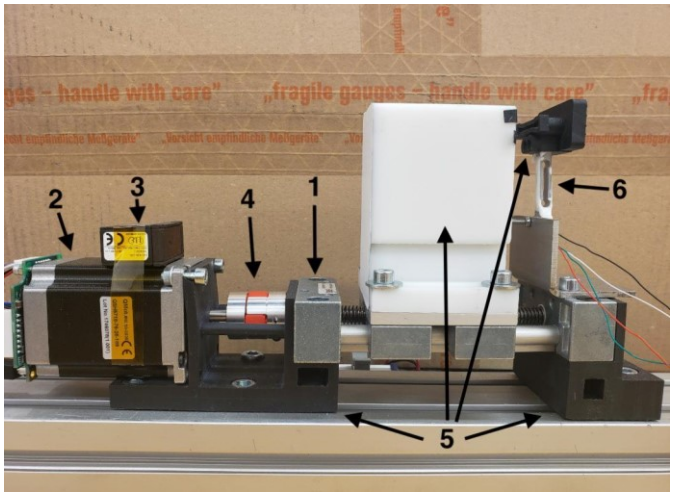

Figure 28: Numerically defined components for Magnetic force sensor device

For the 3D printed parts I used a free CAD programming software called Fusion 360 (Solidworks), which is compatible with Windows and Mac. To print, a Form 2 3D printer was used (13). Once after the parts were printed, it was simply a matter of assembling everything together. The Drylin® lead screw table acts as the mechanism that will allow the movement between permanent magnet (PM) and sample. PM will be located on the part of the lead screw table, inside the 3D printed part, that moves while the load cell will be on the other edge fixed in place. The entire device is securely fixed to a platform for extra reinforcement so that there is little to no vibrations in the system. The optoNCDT laser is used to accurately measure the distances between sample and PM. Both stepper motor and laser are controlled independently via softwares: (TMCL-IDE, optoNCDT).

A very unique and specific 3D part was printed to fit onto the load cell. This part will permit my samples to tightly fit with the exact specimen dimensions plus .5mm for enough space. Figure 29, however, is an image of the exact part with an actual sample fit inside.

Figure 29: 3D printed load cell attachment with sample attached

An important part of this device is the shaft coupler. This part acts as the mechanical connection between the lead screw table and the stepper motor. Without this function there would be no precise way of measuring/controlling the distance between PM and load cell. Therefore, it's imperative that the shaft coupler be tightly fastened and smoothly functioning during operations.

The stepper motor is not only an important component to my device but has also introduced ease of adjusting the lead screw table. It is a 57mm NEMA 23 with a holding torque of 126Ncm with 200 full steps of rotation. This device is optimized for micro-stepping which allows small yet smooth changes in rotational displacement. Lastly, taped on top of the stepper motor, is the laser. Taped because it proved adequate for the stability of the laser sensor. However, this could eventually be optimized for further stability. Its purpose is to accurately measure the distances between the PM and load cell. These measurements will allow for accurate data acquisition.

7.2 FEMM Density Plots

a) 1mm; 8.61581N

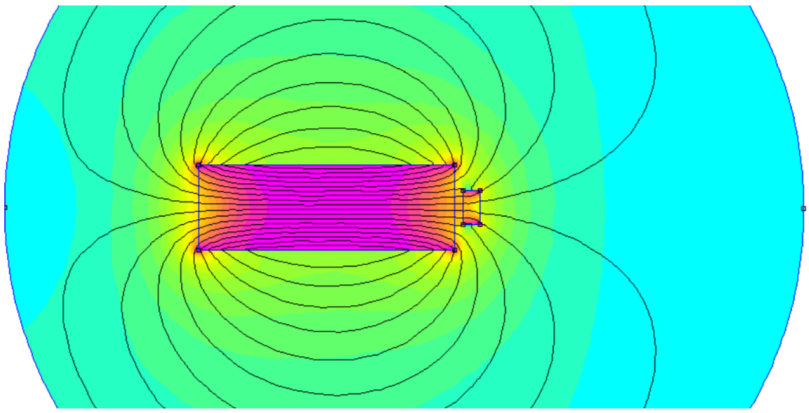

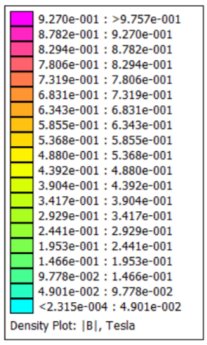

b) 2mm; 6.07113N

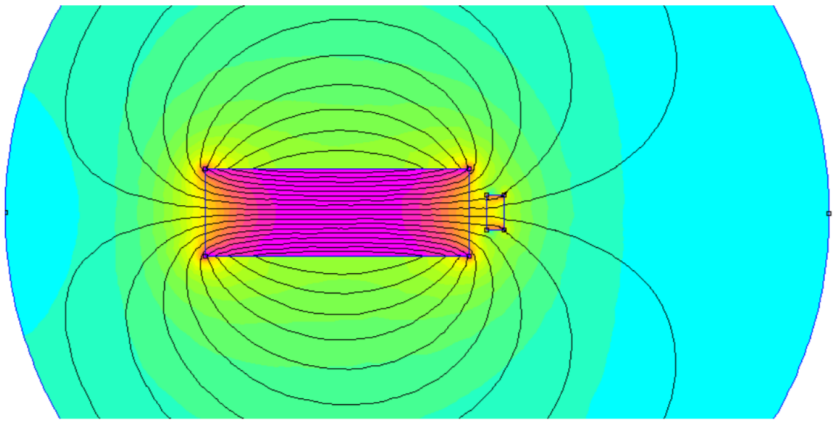

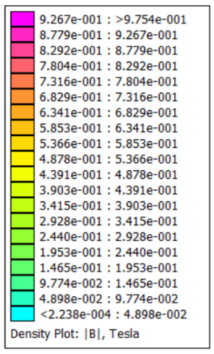

c) 3mm; 4.17205N

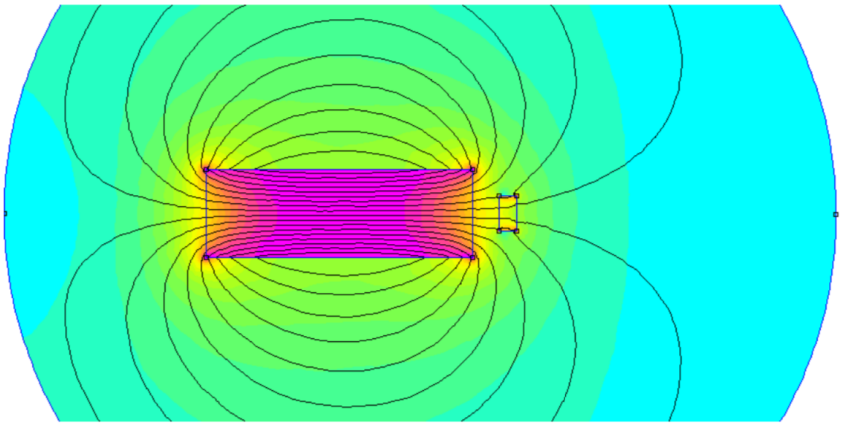

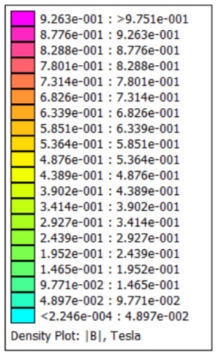

d) 4mm; 2.86516N

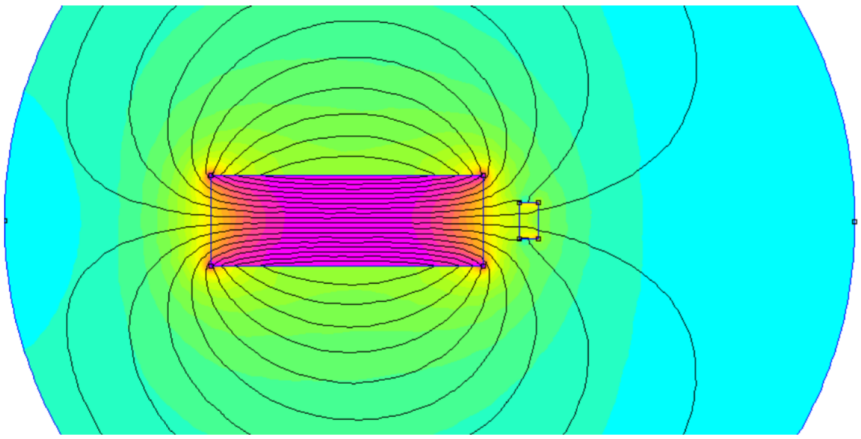

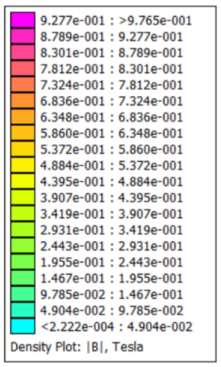

e) 5mm; 1.9839N

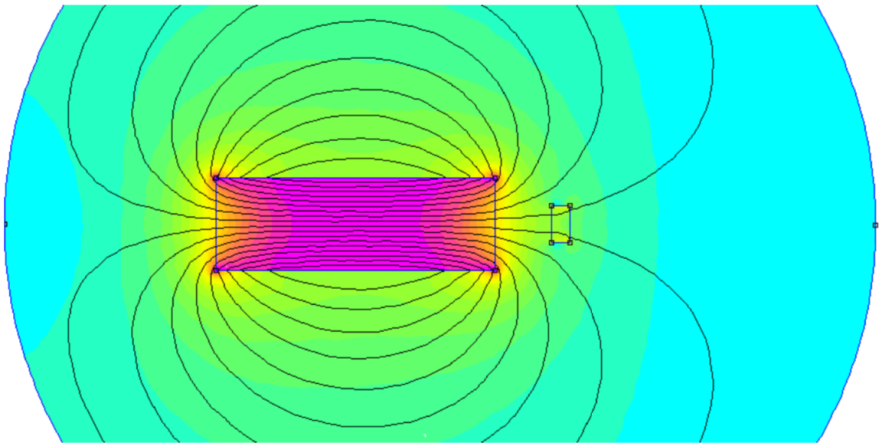

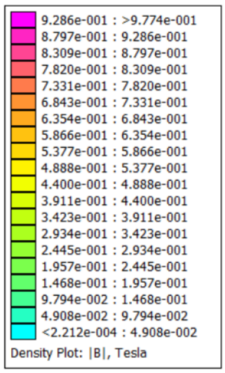

f) 6mm; 1.38674N

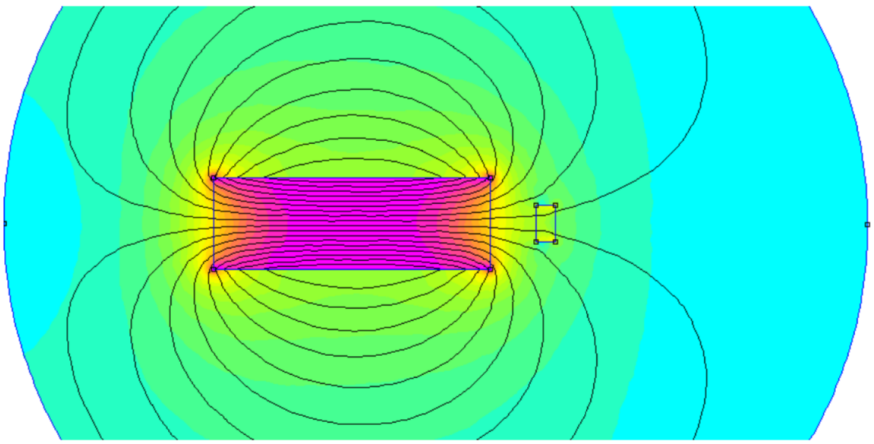

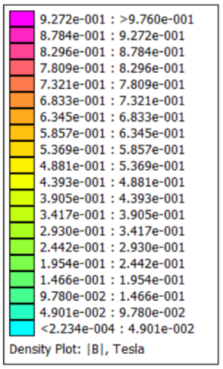

g) 7mm; 0.97814N

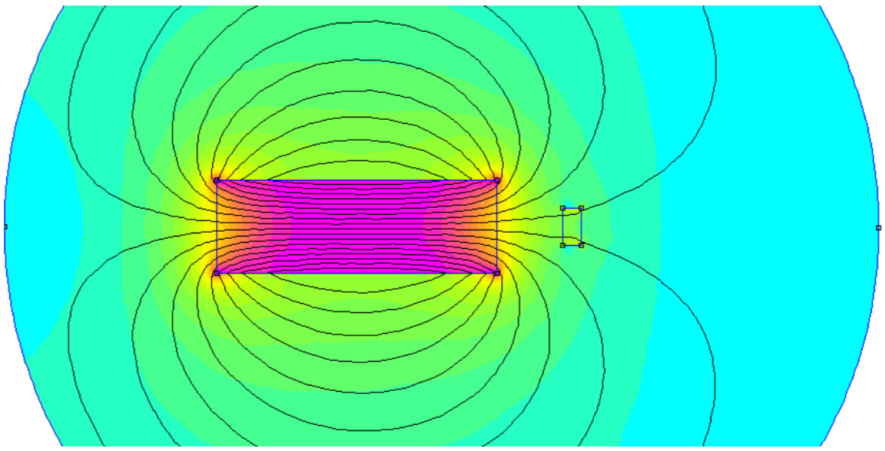

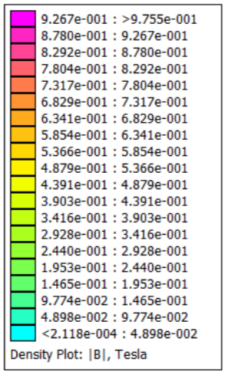

h) 8mm; 0.709581N

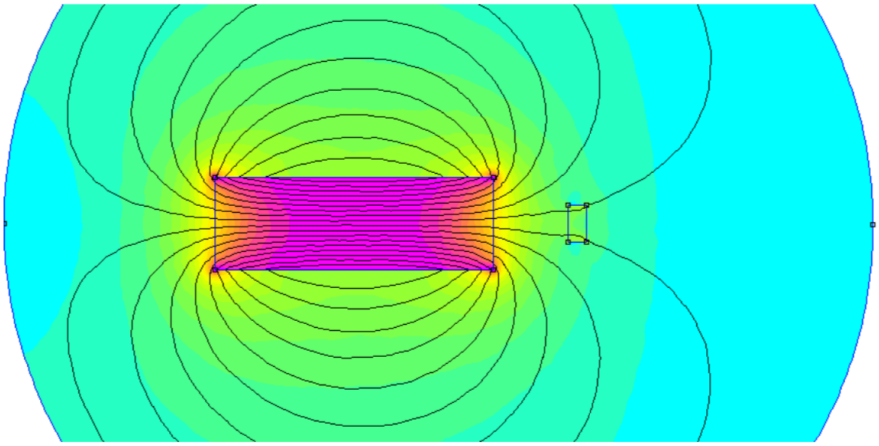

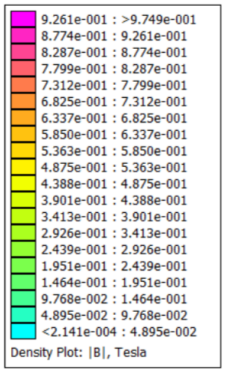

i) 9mm; 0.519109N

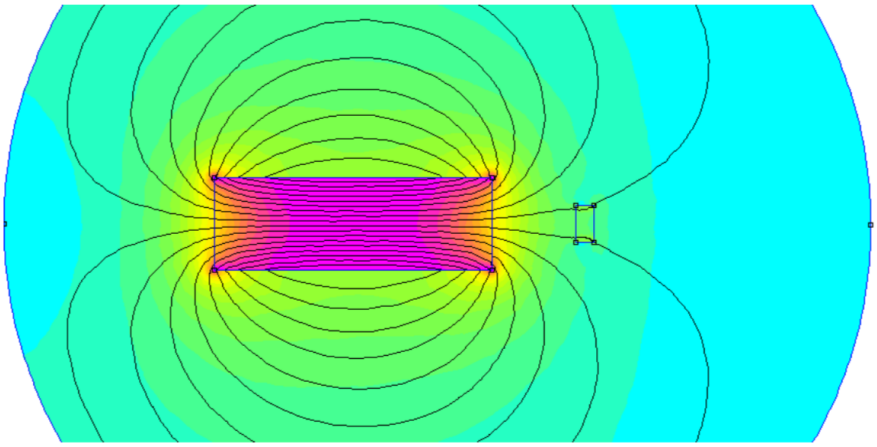

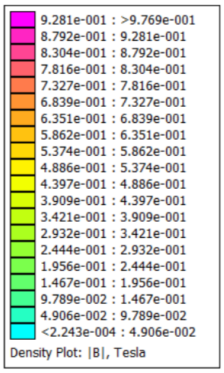

j) 10mm; 0.385565N